HHS Public Access

Author manuscript

Methods Mol Biol. Author manuscript; available in PMC 2020 January 01.

Published in final edited form as:

Methods Mol Biol. 2019 ; 2022: 21–54. doi:10.1007/978-1-4939-9608-7_2.

Force fields for small molecules

Fang-Yu Lin, **Alexander D. MacKerell Jr.***

Computer-Aided Drug Design Center, Department of Pharmaceutical Sciences, School of Pharmacy, University of Maryland, Baltimore, MD 21201, U.S.A.

Summary

Molecular dynamics (MD) simulations have been widely applied to computer-aided drug design (CADD). While MD has been used in a variety of applications, such as free energy perturbation and long-time simulations, the accuracy of the results from those methods depends strongly on the force field used. Force fields for small molecules are crucial as they not only serve as building blocks for developing force fields for larger biomolecules but also act as model compounds that will be transferred to ligands used in CADD. Currently, a wide range of small molecule force fields based on additive or non-polarizable models have been developed. While these non-polarizable force fields can produce reasonable estimations of physical properties and have shown success in a variety of systems, there is still room for improvements due to inherent limitations in these models including the lack of an electronic polarization response. For this reason, incorporating polarization effects into the energy function underlying a force field is believed to be an important step forward, giving rise to the development of polarizable force fields. Recent simulations of biological systems have indicated that polarizable force fields are able to provide a better physical representation of intermolecular interactions and, in many cases, better agreement with experimental properties than non-polarizable, additive force fields. Therefore, this chapter focuses on the development of small molecule force fields with emphasis on polarizable models. It begins with a brief introduction on the importance of small molecule force fields and their evolution from additive to polarizable force fields. Emphasis is placed on the additive CHARMM General Force Field and the polarizable force field based on the classical Drude oscillator. The theory for the Drude polarizable force field and results for small molecules are presented showing their improvements over the additive model. The potential importance of polarization for their application in a wide range of biological systems including CADD is then discussed.

Keywords

Molecular Dynamics Simulations; Additive Force Field; Polarizable Force Field; Drude Oscillator Model; Computer-aided Drug Design; CHARMM

*Corresponding author: alex@outerbanks.umaryland.edu.

Conflict of interest

ADM is co-founder and CSO of SilcsBio LLC.

1 Introduction

Computer-aided drug design (CADD) is assuming an important role in drug development, speeding up the identification of lead compounds as well as facilitating their optimization into new therapeutic agents. Molecular dynamics (MD) simulations based on molecular mechanics have been widely used in CADD to predict binding orientations and provide thermodynamic information, including the prediction of the binding affinity of ligands [1]. MD simulations are based on solving Newton's equations of motion in which the required forces are obtained from a molecular mechanics or empirical force field. Hence, force fields for small organic, drug-like molecules are required and crucial to ensure the accuracy of MD simulations of ligands in drug discovery. MD simulations of ligands alone may be of utility in the context of ligand-based drug design [2–6], or be performed in the presence of the macromolecule, typically a protein, and remaining environment in the context of target-based or structure-based drug design [7–10].

Generating a force field for drug-like ligands represents a significant challenge. Unlike proteins, where the chemical space has relatively limited boundaries (e.g., amino acid side chains and peptide backbone), drug-like molecules have an almost infinite number of possible atom combinations. Although drug-like molecules can be broken down into different pieces, the properties of each chemical group could vary because of the neighboring chemical moieties, especially in conjugated systems. For example, the property of benzene is different from the property of a benzene with a hydroxyl group attached to it. On the other hand, chemical groups such as phenol or imidazole that are linked by extended aliphatic containing moieties do largely maintain their chemical characteristics, allowing for a drug-like molecule force field to be treated as a collection of individual chemical group parts. Thus, the development of accurate organic molecule force fields is challenging and requires large numbers of small model compounds that will act as the parts to be combined to create drug-like molecules.

With the increased interest of modeling and simulation in drug discovery, efforts have been ongoing in the development of drug-like molecule force fields since the early 1980s. Nowadays, the widely used force fields for small molecules are OPLS-All-Atom (OPLS-AA) [11], OPLS3 [12], the CHARMM General force field (CGenFF) force field [13–16], the General AMBER Force Field (GAFF) [17, 18], Merck Molecular Force Field (MMFF) [19–23], and GROMOS [24–28]. These force fields have been actively maintained and regularly improved to include new parameters for a wider range of chemical entities. As manual assignment of parameters for a new molecule requires much experience and is error-prone, algorithms for automatically identifying atom types and generating parameters for molecules have been developed. For example, AnteChamber [18] was designed to generate GAFF and AMBER topologies, and the CGenFF program, accessible through the ParamChem [14, 15] website, was designed to generate CHARMM topologies and parameters based on CGenFF. Other parameter assignment programs include ATB [29] and PRODRG [30, 31] for GROMOS, as well as MATCH [32] and SwissParam [33] for CHARMM.

The majority of force fields for small molecules currently in use are referred to as additive or non-polarizable force fields. These force fields share certain basic characteristics: a potential energy function and the parameters used in the energy function. The term “additive” is based on the use of Coulomb’s law to treat electrostatic interactions with the partial atomic charges, q, being static or fixed, such that the electrostatic energy of the system is simply the sum of all individual atom-atom Coulombic interactions. An example of the typical potential energy function is shown in equation 1.

$$U(r) = \sum_{bonds} k_b(b-b_0)^2 + \sum_{angles} k_\theta(\theta-\theta_0)^2 + \sum_{dihedrals} k_\chi(1+cos(n\chi-\delta)) + \sum_{vdW,i\neq j} \varepsilon_{ij}\left[\left(\frac{R_{min,ij}}{r_{ij}}\right)^{12} - 2\left(\frac{R_{min,ij}}{r_{ij}}\right)^{6}\right] + \sum_{elec,i\neq j} \frac{q_i q_j}{4\pi\varepsilon_0 r_{ij}} \quad (1)$$

Equation 1 includes a simple functional form to describe bonded (or internal) energies and nonbonded energies. Bonded energies come from interactions between covalently bound atoms within three covalent bonds, which include bond and valence angle terms computed based on harmonic stretching and bending potentials, and dihedral angle term expressed as a cosine series expansion. The symbols in Equation 1 are as follows: b_0 and θ_0 are equilibrium values for the bond length and valence angle between atoms, respectively; n is the dihedral multiplicity; δ is the dihedral angle phase; and k_b, k_θ and k_χ are force constants for bonds, angles and dihedral terms. The values of b, θ, and χ are the bond length, valence angle, and dihedral angle for a given atomic configuration. Nonbonded energies are described by van der Waals (vdW) and electrostatic interactions. Calculation of these interactions is normally excluded for atoms connected by one or two covalent bonds (so-called 1–2 and 1–3 pairs, respectively). Energies from vdW interactions are often calculated based on the Lennard-Jones (LJ) 6–12 potential that models electronic repulsion and dispersive interactions. As stated above the electrostatic energies are calculated based on Coulomb’s formula, where each atom is assigned a fixed point charge, also known as partial atomic charges. In Equation 1, r_{ij} is the distance between two atoms i and j, $R_{min,ij}$ is the radius (the distance at which the LJ energy is minimum), and ε_{ij} is the well depth. Once a functional form has been selected, all of the parameters in that functional form for the different types of chemical entities in the force field must be optimized, a process called parametrization.

While the additive force fields have been used for many years and are remarkably successful in biomolecular MD simulations and CADD, there are still inherent limitations in these additive models. One limitation is the lack of explicit treatment of electronic polarizability to model molecules. This limitation is present because the partial atomic charges are fixed, treating the induced polarization in a mean-field average way; however, in reality the electron density of an atom is not static and should be able to adjust in response to the local electric field, such that the electronic polarizability of molecular systems is typically underestimated in condensed phases in most of the additive force fields [34]. To implicitly treat polarization response and give a better representation of the electrostatic properties in condensed phases, a common strategy in additive force fields is to overestimate the gas-

phase dipole moment of the molecule, typically on the order of 20% or more in the dipole moment [35]. This is based on the fact that molecular dipole moments in condensed phases are generally larger than that in the gas phase. For example, the dipole moment of water in the gas phase is 1.9 D [36] whereas in small clusters it is 2.1 D [37] and in the liquid phase 2.9 D [38]. Accordingly, a fixed charge model is unable to obtain accurate properties in different environments, although by implicitly including polarizability through overestimation of the dipole moment has been shown to better model biomolecular systems. While the additive models have shown good agreement with condensed phase properties, such as experimental molecular volumes and enthalpies of vaporizations, this approach is unable to accurately represent the polarization response when molecules are experiencing changes between polar and non-polar environments. For example, in biological systems when a ligand is binding to a protein, or a small molecule is passing through a membrane, the charge distribution of the molecule will change in response to the local electric fields. However, using fixed charges in simulations will not model such variation of electrostatic properties, thereby the accuracy of the simulation using the additive force field is limited.

To solve this problem, a promising approach is to introduce the explicit treatment of electronic polarizability into the potential energy function. Recent advances in polarizable force fields have demonstrated the benefits of explicitly treating the polarization effects, and have yielded improvements and better representations over the additive force fields in a range of system [39–44]. For example, the polarizable models are able to more accurately treat molecular systems in environments with different polar characters, such as the ion distribution near the water−air interface [45–48], ion permeation through ion channel proteins [49–51], water-lipid bilayer interactions [52, 53], protein folding [54], and protein-ligand binding [55–60]. In the remainder of this chapter we first present a short overview of the widely used CGenFF [13, 16] and GAFF [17] additive force fields with the remainder of the chapter focusing on the development of polarizable force fields of small molecules and their improvements in several aspects.

2 Additive CHARMM General Force Field and General AMBER Force Field

2.1 Additive CHARMM General Force Field

CHARMM General Force Field (CGenFF) [13, 16] is a force field developed for drug-like molecules and is compatible with CHARMM36 additive biomolecular force field [61–76]. It is associated with of a wide range of model compounds, which were highly optimized based on a standard CGenFF parametrization protocol [13]. The protocol involves parametrizing partial atomic charges targeting QM dipole moments and water interaction energies, LJ parameters targeting experimental condensed phase properties and bonded parameters targeting QM calculated geometries, vibrational spectra and dihedral potential energy scans. More importantly, the parametrization philosophy in CGenFF focuses on the transferability among the model compounds rather than over-fitting of the parameters, such that the developed parameters for the small molecular will be appropriate building blocks for larger drug-like molecules.

The CGenFF program [14, 15] automatically provides CGenFF parameters for a molecule. This process includes atom typing, followed by parameters and charges being assigned in an

automated fashion by analogy to those in the highly optimized small model compounds existing in CGenFF. The first step of assigning parameters is to assign atom types for atoms of a given molecule. This is performed by the “atom typer” module in the CGenFF program. In practice, the atom typer will first retrieve the information of atoms in the molecule, the connectivity pattern of these atoms, and the bond types between these atoms, which are typically obtained through mol2 format file. Then, the assignment of the atom types is determined through a decision tree based on a rule file that has many subcategories for different chemical properties, such that according to the decision tree, the atom typer will proceed from the main category to the next subcategory until the condition for each atom is satisfied leading to assignment of the atom type. Next, the CGenFF program will assign bonded parameters and charges to the given molecule based on those atom types. However, as existing bonded parameters are often not present in CGenFF for a given connectivity of atoms, the missing bonded parameters are identified by analogy based on the similarity between the atom types that define the parameters. Charges are assigned through a bond-charge increment scheme, similar to that implemented in MMFF94 [19–23]. Notably, in addition to single charge increment for each bond, there are two charge increments for each angle and three charge increments for each dihedral angle in the CGenFF program. While such an approach requires the optimization of the charge increments, it has the advantage of capturing the inductive and resonance effects as well as improve transferability between the dihedral parameters and the 1–4 electrostatic interactions. Finally, a “penalty score” is returned for bonded and charge parameters that are assigned based on analogy, allowing users to estimate the quality of the force field for the given molecule, such that parameters with small penalties are assumed to be of better accuracy versus those with high penalties. However, it should be emphasized that the penalties are based on analogy rather than based on the reproduction of specific target data, such that parameters with higher penalties may be of suitable accuracy while parameters with low or zero penalties may be of limited accuracy due to their being in a chemical connectivity not included in the original parametrization. Accordingly, it is suggested that when the parameters for a given molecule are critical, such as with a lead compound that will undergo extensive optimization, the user should perform QM calculations to determine if the geometry and conformational energies are satisfactory. This effort could include comparison of the empirical and QM dipole moments as well as interactions with water. Information on our webpage (http://mackerell.umaryland.edu/) as well as tools such as the Force Field Toolkit (ffTK) [77], or General Automatic Atomic Model Parametrization (GAAMP) utility [78] can be accessed to facilitate such a process.

2.2 Additive General AMBER Force Field

General AMBER Force Field (GAFF) [17] is designed for a wider range of organic molecules that are compatible with existing AMBER force fields which were developed primarily for proteins and nucleic acids [79, 80], with subsequent extensions to carbohydrates [81–83] and lipids [84]. In the original version of GAFF [17], there were 33 basic atom types and 22 special atom types to cover most of the chemical space having the elements H, C, N, O, S, P, F, Cl, Br, and I. The atom types in GAFF are determined based on the element, hybridization, aromaticity, and chemical environment. In practice, for each atom the match is performed through each definition string; so when a successful match is

achieved, the atom type is assigned. The bonded parameters are derived based on empirical functions associated with reference data including QM results, empirical rules and crystal structures. The charges in GAFF are computed from QM *ab initio* (i.e. HF/6–31G* RESP charge) [80, 85, 86] or AM1-BCC semi-empirical model [87]. Thus, the charges in GAFF are explicitly determined for each molecule based on the QM method applied. Accordingly, the charge determination requires a significant amount of computational time, which possibly becomes a bottleneck in high-throughput applications requiring a large numbers of molecules. This contrasts CGenFF where the charge assignment is instantaneous. In addition, GAFF does not supply any metric of the quality of the assigned parameters.

3 Polarizable Force Fields

With the increasing focus on the polarization response in simulations, several polarizable force fields have been developed. Currently, polarizable functional forms used in polarizable force fields can be classified into three categories: the fluctuating charge model, the induced dipole model, and the classical Drude oscillator model. These models are briefly introduced below. In all three models, the remainder of the functional form of the potential energy function is largely the same as in additive force fields, though variations are seen.

3.1 Fluctuating charge model

In the fluctuating charge model, the calculation of electrostatic energies involves the partial atomic charges on the molecule redistributing in response to the electric field from the environment such that the molecular dipole changes. The redistribution of the charges between atoms is based on the relative electronegativity and hardness of each atom (*see* Note 1), while the overall charge on the molecule is maintained. This model has been used in the universal force field (UFF) developed by Rappe et al. [88], force fields developed by Berne, Friesner, and co-workers [89–91], and in the CHARMM fluctuating charge (FQ) force field [92, 93]. However, one limitation of this model is its inability to describe the out-of-plane polarization directly for planar systems, such as water or conjugated molecules, which is due to electrons only being able to redistribute between atoms in the plane of the molecule. A strategy to solve this problem is to add out-of-plane virtual sites so that the redistribution of the charge is possible in the orthogonal direction to yield the out-of-plane polarization. Another limitation is the application in monatomic ions, as the redistribution of the charge is not possible for a single charge site. Thus, in early studies of ion solvation with the fluctuating charge model for water, a modified Drude oscillator (described below) was used for the monatomic ions to model the electronic polarization [94].

3.2 Induced dipole model

In this representation, inducible dipoles are added to atomic sites. As shown in equation 2, the dipole moment (μ_i) induced on the atom (i) is proportional to its atomic polarizability (α_i) and the total electric field at that site. The total electric field includes electrostatic fields

[1] Electronegativity is the attraction of an atom for electrons. Hardness is the work needed to transfer charge between atoms.

E_i^0 and E_i^p, where E_i^0 is created on the atom (i) by the permanent charges, and E_i^p is created by the other induced dipoles from the rest of the atoms in the system (*see* Note 2).

$$\mu_i = \alpha_i\left(\mathbf{E}_i^0 + \mathbf{E}_i^p\right) \quad (2)$$

Thus, the contribution of the polarization energy, U_{pol}, to the total nonbonded energy is described as:

$$U_{pol} = -\frac{1}{2}\sum_i \mu_i \mathbf{E}_i \quad (3)$$

The induced point dipole model has been used in several polarizable force fields, including OPLS/PFF [95], AMBER [96–100], and PIPF [101] as well as force fields developed by Berne, Friesner, and co-workers [95, 102], in the water, ion, and small molecule force field of Dang and coworkers [103–105], and others [106–109]. Ren and Ponder combined the induced dipole model with atomic multipoles through the quadrupole moments in the treatment of the electrostatic interactions in the context of the AMOEBA force field [110–112]. However, the induced dipoles are typically determined by a self-consistent field (SCF) iterative procedure followed by the calculation of the electrostatic energy of the system from the charge–charge, charge–dipole, and dipole–dipole interactions, representing a bottleneck associated with the demanding computational time. To reduce computation, Wang et al. proposed the iAMEOBA [113] approach with induced dipoles initially set to zero such that the response of induced dipoles to the permanent electrostatics has no mutual induction, thereby avoiding the iterative SCF step. Recently, Albaugh et al. developed a new approach, (iEL/0-SCF) [114] based on iEL/SCF Lagrangian scheme [115], from which the auxiliary induced dipoles serve as initial guesses for the real induced dipoles and stay close to the Born–Oppenheimer surface to achieve a SCF-less calculation. An interesting alternative has been introduced by Brooks and coworkers in which the induced dipoles are treated using perturbation theory [116] and the multipoles are treated using spherical harmonics [117]. That model, term MPID, was recently shown to be equivalent to the Drude model in a study in which the Drude parameters were mapped on to the MPID formalism [118].

3.3 Classical Drude Oscillator Model

The classical Drude oscillator model is also referred to as the Shell or charge-on-spring model. In the Drude oscillator model, explicit polarization is introduced by attaching a charged auxiliary particle (the Drude oscillator or particle) with a harmonic spring to the core (i.e. nuclei) of each polarizable atom, which allows the atomic dipoles to adjust in response to the surrounding electronic field by simply minimizing the position of the Drude particles with the atomic core fixed (Figure 1). This is analogous to the SCF calculation in

2. The total electric field in induce dipole model is determined self-consistently via an iterative procedure that minimizes the polarization energy via optimization of the atomic dipoles with the atomic nuclei fixed or via the extended Lagrangian method in the context of MD simulations [115, 222, 223].

the context of the Born-Oppenheimer approximation. The electrostatic energy is then obtained from the Coulombic interactions between the atomic and Drude charges (equation 4). Accordingly, the Drude oscillator model retains many of the pair-wise features of the functional forms as those in the additive models (equation 1), but the potential energy function is modified to further include the energy results from the Drude particles thereby explicitly treating polarizability. In equation 4, q_i and q_j are the charges on atom i and j, $q_{D,i}$, and $q_{D,j}$ are charges on the respective Drude particles, r_i, r_j, $r_{D,i}$ and $r_{D,j}$ are their locations.

$$E_{\text{elec,Coulombic}} = \frac{1}{4\pi D}\left(\sum_{i\neq j}\frac{q_i q_j}{\|\boldsymbol{r}_i-\boldsymbol{r}_j\|}+\sum_{i\neq j}\frac{q_{D,i}q_j}{\|\boldsymbol{r}_{D,i}-\boldsymbol{r}_j\|}+\sum_{i\neq j}\frac{q_{D,i}q_{D,j}}{\|\boldsymbol{r}_{D,i}-\boldsymbol{r}_{D,j}\|}\right) \quad (4)$$

In the Drude model the isotropic atomic polarizability, α, is defined based on the magnitude of the charge on the Drude particle, q_D, and the force constant, K^D, on the spring attaching the Drude particle to the atomic core as shown in equation 5.

$$\alpha = \frac{{q_D}^2}{K^D} \quad (5)$$

Thus, the value of α will determine the charge assigned to the Drude particle (q_D), and the total partial atomic charge on the atom (q_A) will be $q_A=q-q_D$, where q is the charge assigned to the atomic core. From this description, polarization is determined by a pair of point charges (q_A and q_D) separated by a variable displacement, d, between the Drude particle and the atomic core, which is able to adjust in response to the electric field, **E**, according to the equation 6:

$$\mathbf{d} = \frac{q_D \boldsymbol{E}}{K^D} \quad (6)$$

The induced atomic dipole, μ, will be calculated as:

$$\mu = \frac{{q_D}^2 \boldsymbol{E}}{K^D} \quad (7)$$

The electrostatic component of the potential energy function therefore includes Coulombic electrostatic interactions between atom-Drude and Drude-Drude pairs as shown in equation 4 above and a harmonic self-polarization term, U_{self}, calculated using:

$$U_{self} = K^D \mathbf{d}^2 \quad (8)$$

The resulting total potential energy function, U, in the polarizable force field will become an extension of the additive energy functional form with U calculated as:

$$U(\mathbf{r}, \quad \mathbf{d}) = U_{bond}(\mathbf{r}) + U_{LJ}(\mathbf{r}) + U_{elec}(\mathbf{r}, \mathbf{d}) + U_{self}(\mathbf{d}) \quad (9)$$

where U_{bond} indicates the bonded internal energy terms (e.g. bonds, angles, and dihedrals), U_{LJ} is the LJ energy term, U_{elec} represents all the Coulombic electrostatic interactions (e.g. interactions between atom-atom, atom-Drude, and Drude-Drude pairs), and the self-polarization U_{self}. The Drude particles in the CHARMM Drude polarizable force field are only associated with non-hydrogen atoms, which has been shown to be sufficient to reproduce molecular polarizabilities and to minimize computational cost in the calculation of electrostatic interactions [119].

The representation of U_{self} in equation 8 treats polarization isotropically, where the K^D is the scalar value of harmonic force constant. To improve nonbond interaction as a function of orientation, the polarization on the Drude particle can be treated anisotropically. This is achieved by expanding the scalar K^D to a tensor K^D, as shown in equation 10 such that the anisotropic form of U_{self} becomes:

$$U_{self} = \frac{1}{2}\left(K_{11}^{D}\mathbf{d_1}^{\ 2} + K_{22}^{D}\mathbf{d_2}^{\ 2} + K_{33}^{D}\mathbf{d_3}^{\ 2}\right) \quad (10)$$

where $\mathbf{d_1}$, $\mathbf{d_2}$, $\mathbf{d_3}$ are the projections of the Drude particle-atom displacement vectors on the orthogonal axes defined based on the local molecular frame, and K^D is a tensor with off-diagonal elements set to zero. Additionally, lone pairs can be added to further improve the description of electronic distribution around hydrogen bond acceptor atoms (Figure 1) [120]. The combination of anisotropic polarization and lone pairs results in an improved description of functional groups acting as hydrogen-bond acceptors [120].

Another difference from the additive model is that the Drude model includes explicit treatment of induced dipole–dipole interactions for 1–2 and 1–3 atom pairs. This allows for better treatment of molecular polarizabilities as first introduced by Thole. However, as the induced dipoles are treated as point charges that are in close proximity (Figure 2) and, therefore, not well modeled using Coulomb's law, those electrostatic interactions are screened by a Thole-like screening function S_{ij} [121]:

$$S_{ij}\left(r_{ij}\right) = 1 - \left[\left(1 + \frac{\left(t_i + t_j\right)r_{ij}}{2\left(\alpha_i\alpha_j\right)^{1/6}}\right)\right]\exp\left[\frac{-\left(t_i + t_j\right)r_{ij}}{\left(\alpha_i\alpha_j\right)^{1/6}}\right] \quad (11)$$

where r_{ij} is the distance between atoms i and j, α_i and α_j are respective atomic polarizabilities, t_i and t_j are the respective atomistic Thole screening factors that dictate the degree of scaling. The use of atom specific Thole screening factors along with the 1–2 and

1–3 interactions is particularly useful with respect to the reproduction of molecular polarizability tensors, as shown schematically in Figure 2.

While the Drude model has performed well, accurately reproducing QM and experimental target data in a variety of systems, it has been observed that the hydration free energies were shown to be overestimated compared to the experimental values. One explanation for this is that the Lorentz-Berthelot combining rules [122] (equation 12 and 13) are inadequate to describe the LJ contributions to the solvation energies.

$$R_{min,\,ij} = \frac{\mathrm{R_{min}}}{2},\mathrm{i} + \frac{\mathrm{R_{min}}}{2},\mathrm{j} \quad (12)$$

$$\varepsilon_{ij} = \sqrt{\varepsilon_{\mathrm{i}} \times \varepsilon_{\mathrm{j}}} \quad (13)$$

To allow for a more accurate reproduction of hydration free energies, the strategy of using “atom pair-specific LJ parameters” [123] between the water oxygen and select solute non-hydrogen atoms was developed to override the standard LJ combining rules. Thus $R_{min,\,ij}$ and ε_{ij} of an atom pair are not assigned through the combining rules (equation 12 and 13) but they are specified directly according to the atom pair-specific LJ parameters (NBFIX in CHARMM nomenclature). By utilizing the atom pair-specific LJ parameters, the hydration free energies of the molecules could be improved without affecting pure solvent properties and other molecular interactions.

One limitation of the Drude model, as well as other polarizable models, is the possibility of over-polarization. With the Drude model, this occurs when the Drude particle is displaced far from its parent atomic core, resulting in unphysically large interaction energies leading to the so-called polarization catastrophe. To prevent this from happening, a “hard-wall constraint” [124] is introduced to prevent Drude particles from moving further from a specific displacement, typically is 0.2 Å, from the atomic core. The Drude model also includes an additional anharmonic term representing a restoring force to prevent excessively large excursions of the Drude particle away from the atom [47, 125], thereby reducing the polarizability of atoms at high electric field. This latter term is not commonly used in the current version of the Drude force field.

As in other polarizable models, the calculation based on the SCF scheme would be time-consuming in simulations. To perform simulations more efficiently, Lamoureux and Roux developed an extended Lagrangian approach for the Drude model [126], in which each Drude particle is given a small mass (0.4 amu) that is subtracted from the parent atom (i.e. total mass of the Drude–atom pair is still equal to the atomic mass). As the Drude particles are now included in the equations of motion, typically a 1 fs time step is used in simulations to prevent large forces associated with the Drude particles, which would be an inherent limiting factor with respect to the computational time. Drude polarizable simulations using

the extended Lagrangian are approximately a factor of two slower due to the additional nonbond calculations versus an additive model, with an additional factor of two present if integration time steps of 1 versus 2 fs are used for the Drude and additive models, respectively.

3.4 Scope of the Most Widely used Polarizable Force Fields

The current scope of the most widely used polarizable force fields is summarized in Table 1. The AMBER polarizable force field has been developed for the study of ions [96, 98], and neat liquid properties of water methanol, and N-methylacetamide [97]. A more extended force field, AMBER ff02, was released including parameters for acetamide, dipeptides, and nucleic acid bases and it is available for simulations on proteins/peptides and nucleic acids [99, 100]. CHARMM fluctuating charge (FQ) force field has been developed for several biomolecules including proteins [92, 93], lipids [127], and selected carbohydrates [128]. In addition, this force field has been applied to the study of ligand binding to lysozyme [129], ion solvation [130], and lipid bilayer permeability [131]. Parameters for drug-like small molecules have not been reported with the AMBER or CHARMM FQ models.

AMOEBA has been developed for water [110], ions [132, 133], and a fully functional model for protein [112]. While the quality of parameters for nucleic acid has not been reported in the literature, they are available in the Tinker package [134] via the website at http://dasher.wustl.edu. Currently, AMOEBA polarizable parameters of several small organic compounds containing biologically important functional groups have been presented, including alkanes, alcohols, amines, sulfides, aldehydes, carboxylic acids, amides, aromatics [135], and chloromethanes [136]. While parameters have not been reported for simulations on carbohydrates or lipids, AMOEBA has already demonstrated its success in various molecular systems where polarization is critical, including the study of liquid water [110, 137], ion solvation properties [132, 138, 133], computational X-ray crystallography [139], ligand-bindings [140], *N*-methyl-acetamide dimers, alanine dipeptide conformational study [141], and binding free energies calculations for small ligands [55, 56, 142].

MacKerell, Roux and co-workers have developed the Drude polarizable force field for a range of molecular systems as well as atomic ions. Parameters have been published for water models [143, 144], ions [47], and a range of small molecules representative of biological macromolecules [119, 145–156], and more recently of halogenated species [157]. Force field parameters have also been published for biomolecules including carbohydrates [158–161], proteins [162], DNA [163–166] and selected lipids [124, 167]. These biomolecular parameters have been used in a number of application studies, showing the role of explicit treatment of electronic polarization in the cooperativity of both peptide folding and peptide unfolding [168] as well as base flipping in DNA [169]. Other interesting results include the sensitivity of the solution structure of DNA to different types of monovalent ions [170]. Current efforts on the Drude biomolecular force field involve additional refinements, which are anticipated to yield improved models of increased accuracy that will yield an optimized picture of the physical properties of macromolecules and their relationship to their structure, dynamics and function. A more detailed description of the small molecules treated by the Drude force field is given below.

4 Current Status of Drude Polarizable Force Field for Small Organic Molecules

In the following sections a detailed description of the various classes small molecules in the Drude force field that have been developed to date will be presented. These molecules were primarily selected as the basis for extension of the force field to larger entities, such as protein [162], nucleic acid [44, 163, 164, 166], lipid [124, 167], and carbohydrate [160]. More recent development of Drude parameters for halogens combined with the small molecules represent the initial molecular building blocks that will lay the foundation for a Drude General Force Field (DGenFF) for molecules of medicinal chemistry interest.

4.1 Alkanes

Parametrization of alkanes are essential as they serve as model compounds for the aliphatic groups, which are major components of biological macromolecules, including lipid tails, amino acid side chains, and the majority of carbohydrates. While additive models have been developed in a wide range of force fields and have shown great utility in studying a variety of systems, the additive models yield a systematic underestimation of alkane dielectric constants, which is due to their inability to account for the high-frequency electronic oscillating field that contributes to the optical dielectric constant, leading to dielectric constants for pure alkanes of approximately 1 (*see* Note 3). Accurate treatment of the dielectric constants, which should be approximately 2, is critical in simulating biomolecular systems given that the free energy of solvation scales with $(1 - 1/\varepsilon)$, where ε is the dielectric constant of the environment. Thus, even a small underestimation of alkane dielectric constants would cause a significant impact on the treatment of solvation in nonpolar environments, particularly for compounds that need to pass through the hydrophobic region of lipid bilayers when they are crossing the membrane. Accordingly, an accurate force field for alkanes that is able to properly treat the dielectric constant is required. The Drude polarizable model for alkanes, including ethane, propane, butane, isobutene, and pentane, meets this need as the dielectric constants of those pure liquids are in good agreement with the experimental values [145].

When developing the Drude alkane electrostatic parameters, the ability to readily transfer those parameters to more complex molecules was considered. Transferability was insured by imposing a restraint on the charges of carbons (q_C) and hydrogens (q_H) based on $q_C = -xq_H$, where x is the number of hydrogen atoms, such that the charges on CH_x groups would be neutral. A polarizability scaling factor of 1, which is different from the polarizable scaling factors (0.70~0.85) for other small molecules [119, 146–155], yielded good

3. The static dielectric constant, ε, is calculated from the dipole moment fluctuations of the entire simulation system according to:

$$\varepsilon = \varepsilon_\infty + \frac{4\pi}{3\langle V\rangle K_B T}\left(\left\langle M^2\right\rangle - \langle M\rangle^2\right)$$

where M is the total dipole moment of the cubic simulation system, $\langle V\rangle$ is the average volume of the cubic unit cell, and ε_∞ is the high-frequency optical dielectric constant which was estimated from the Clausius-Mossotti equation [224].

agreement with experimental observables. The model was able to reproduce experimental enthalpies of vaporizations (ΔH_{vap}), molecular volumes (V_m), hydration free energies (ΔG_{hydr}), NMR relaxation times, and particularly the static dielectric constants. The accurate reproduction of the static dielectric constants was an important outcome. For example, the Drude polarizable alkane model produced significantly better agreements with experimental dielectric constants that were ranging from 1.71 to 2.13 for alkane series, whereas the additive model produced nearly uniform values of 1.0 regardless of different alkyl chain length.

The Drude alkane force field was originally parametrized by including long-range LJ interactions using an isotropic correction for pure solvents and in aqueous solution [124]. However, isotropic treatment of long-range LJ interactions is inappropriate for modeling anisotropic systems such as alkane/air interfaces [171], becoming a significant problem in modeling the structural and thermodynamic properties of lipids. To overcome this limitation, Leonard et al. [172]. have applied the Lennard-Jones particle-mesh Ewald (LJ-PME) method [173] (*see* Note 4) to better model the LJ contribution in anisotropic systems. Their results showed the Drude polarizable model with LJ-PME to have improved agreement across various experimental quantities, such as density, isothermal compressibility, surface tension, viscosity, translational diffusion, and ^{13}C T_1 relaxation times of long-chain pure alkanes. Moreover, the Drude results are systematically closer to the experiment than the CHARMM36 additive counterpart. Accordingly, the updated polarizable model for these alkanes is expected to improve the accuracy of modeling the hydrophobic environments, such as lipid bilayers.

4.2 Ethers

Ether moieties are substructures of important functional groups in biological molecules, such as furanoses, including ribose and deoxyribose, and pyranoses. Accordingly, the accuracy of the ether parameters lays the foundation for extending the polarizable force field to carbohydrates and nucleic acids. Ethers are generally considered as relatively nonpolar due to the nonpolar aliphatic groups, while the polar oxygen atoms are capable of participating in hydrogen bonds and ion coordination. Therefore, the development of the force field for ethers requires attaining the right balance between dispersion, electrostatic and repulsive forces. Vorobyov et al. developed the initial Drude polarizable model for linear and cyclic ethers [150]. The developed ethers includes tetrahydrofuran, tetrahydropyran, dimethyl ether, methyl ethyl ether, diethyl ether, and 1,2-dimethoxyethane. To ensure transferability, the parameters for cyclic ethers were developed first then subsequently transferred to a series of linear molecules. One of the significant outcomes of the ether polarizable model was the ability to more accurately treat the polar character in different environments. In the additive model, the dipole distributions are nearly identical from the gas to aqueous phase for THF and DEE (~ 2 and 1.8 D, respectively). In contrast, the differences of dipole distributions in the different environments in the polarizable model are more significant, with an obvious increase from the gas to aqueous phase. These

[4]Lennard-Jones particle-mesh Ewald (LJ-PME) method [173] extends the particle-mesh Ewald (PME) method [225, 226] to long-range LJ interactions. LJ-PME is suitable for use with anisotropic systems, such as lipid bilayers and monolayers.

observations indicated that the polarizable models are more responsive to the polarity of the environment. Another key outcome in the polarizable model for ethers is their agreement in relative energies of various conformations and their corresponding dipole moments [147], which reflects the ability of the polarizable model to accurately model the electronic properties in various conformations. However, the dielectric constants of the neat liquid cycloalkanes and ethers were still not optimal and systematically underestimated, with an average percentage difference of −13% compared to the experimental values. As a result, Baker et al. reparametrized the model including the use of atom-type-dependent Thole screening factors (t, in equation 11) [119] and applied a scaling factor of 0.85 for the gas molecular polarizabilities. The new model significantly improved the reproduction of the dielectric constants, while maintaining good agreement of properties from the previous model as well as other experimental and QM data, reinforcing the sensitivity of the atomic polarizability parameters.

4.3 Alcohols

Alcohol moieties are functional groups that are ubiquitous in biological molecules, such as amino acid (e.g. serine, threonine, and tyrosine), nucleic acids (e.g. 2′- and 3′-hydroxyl groups), carbohydrates, and lipids. As alcohols consist of both polar and nonpolar components, the hydration of alcohols involves hydrophobic and hydrophilic interactions. Therefore, proper treatment of electronic polarization is required to ensure the accurate description of the balance of the hydroxyl-water and aliphatic-water interactions. While a number of nonpolarizable models for alcohol-containing molecules are available, the gas-phase dipole moment of alcohols were overestimated by approximately 40% to implicitly treat the condensed phase polarization effects [149]. A polarizable alcohol force field using the Drude oscillator model was initially presented by Noskov et al. [146] to elucidate the hydrophobic hydration in water−ethanol mixtures. Subsequently, a more generalized parameter set for alcohols was developed by Anisimov et al, including a larger series of primary and secondary alcohols (e.g. methanol, ethanol, 1-propanol, 1-butanol, secondary alcohols, 2-propanol, and 2-butanol.) [149]. The updated model added lone pairs on the hydroxyl oxygen atom and introduced atom pair-specific LJ parameters for alcohol oxygen atoms with water oxygen atoms. The polarizable model developed based on the training set molecules was found to present a significant improvement over the additive model in all cases for ΔH_{vap} and ΔG_{hydr}, and dielectric constants. Notably, the Drude polarizable model has shown the ability to capture the response of the molecular dipole moments in response to different environments. The dipole moments of ethanol and 2-propanol shifted from low dipole moments in the gas phase to much higher values when solvated in aqueous solution, in agreement with previous theoretical calculations [174]. Whereas the dipole moments obtained from the additive model were largely unchanged in the simulations in gas phase, pure solvent, and aqueous systems. Moreover, small variations of the dipole moment of water molecules hydrating alcohols were observed as a function of distance, showing that the intermolecular interactions between water and alcohols would be dictated by their mutual polarization. These results clearly indicate that the polarizable model is more applicable in modeling the dynamics of molecules containing hydroxyl group in different environments than additive force fields.

4.4 Amides

As amide moieties comprise protein backbones and the side chain of asparagine and glutamine, as well as being components of carbohydrates, an accurate model for amide group is critical for the development of a polarizable protein force field, motivating efforts to parametrize amide-containing model compounds [119, 154]. The initial Drude polarizable model for amides reproduced a wide range of gas-phase QM and condensed-phase experimental data. Particularly, the amide polarizable model was able to reproduce the high dielectric of neat N-methylacetamide (NMA, 100 at 373 K), whereas the additive model yielded a 70% underestimation of the dielectric constant, indicating that the mean-field approximation in the additive model is limited to account for the induced electronic polarization [175]. Two factors could account for this large dielectric constant in the polarizable model. One is the increased average NMA dipole moment in the neat liquid than in the gas phase. The other is the intermolecular hydrogen bonding (Figure 3) that enhances the orientational alignment of the molecular dipoles. This is consistent with the calculated Kirkwood G_K factor [176] (*see* Note 5) that G_K was considerably larger in the polarizable model ($G_K = 4.6$) than in the additive model ($G_K = 3.0$). This result indicates that the inclusion of explicit electrostatic polarization is expected to lead to a greater accuracy in modeling of hydrogen bonding interactions. However, the early model for amide-containing compounds primarily focused on neat liquid simulation properties. An updated model for NMA and acetamide [154] was presented to further assess the properties of the amide series in aqueous solution in greater detail. While the value of the dielectric constant was significantly smaller than the previously reported value, there was a better balance of the solute-solute, solvent-solute, and solvent-solvent interactions in the updated models. Such a balance is a crucial factor for applying the model in the Drude polarizable protein force field as the relative stability of helical vs. sheet vs. random coil conformations and protein conformational dynamics [177] are related to the balance of protein intramolecular and protein–solvent interactions.

4.5 Aromatic and Heteroaromatic Systems

Aromatic rings are commonly used in drug design as they make hydrophobic contributions to binding, allowing them to participate in hydrogen bonding and are able to participate in π interactions [178]. Therefore, the development of an aromatic polarizable force field would be useful in drug-like molecules [179] as well as serve as building blocks for parametrizing phenylalanine and tyrosine in the development of protein force field and the nucleic acid bases. Benzene and toluene parameters were initially developed [151] followed by parameters for heteroaromatics [151] and subsequently nucleic acid bases [163–166]. While many of the dynamic features of the benzene and toluene liquids are similar between the polarizable and additive models, the polarizable model is more accurate in reproducing the experimental dielectric constants. The additive force field dielectric for benzene was close to 1.0, considerably lower than the experimental value of 2.3 for benzene and 2.4 for toluene, whereas dielectric constants obtained from the Drude model yielded better agreement. In

[5] The Kirkwood factor (G_K) [176] is a measure of the orientational correlation with molecular dipoles. Configurations that have parallel dipole alignment lead to $G_K > 1$, and for uncorrelated dipoles, $G_K = 1$. Therefore, that larger G_K indicates a greater degree of cooperative dipole alignment.

parametrizing aromatic molecules, one important feature to be reproduced is the interactions between the π electron system on the aromatic rings and water (*see* Note 6) [180, 181]. From the radial and spatial distribution functions of aqueous solutions of benzene and toluene, subtle differences of hydration shells were observed between the two models. The Drude polarizable model produced a more defined population of water molecules at 3.5 Å above the ring than the additive model, which indicates that the Drude polarizable model is more capable of capturing the out of plane π-stacking interaction between the aromatic ring and water, providing a more physical description of hydration of aromatic moieties. Further improvements in the polarizable benzene model were made by Esam et. al. with respect to cation−π interactions [182]. In their study, QM interaction orientations and energies were better reproduced by introducing a virtual particle in the center of the benzene ring with the use of atom pair-specific LJ parameters.

A series of heterocyclic aromatic compounds (e.g. pyrrole, imidazole, pyridine, pyrimidine, indole, and purine) based on Drude polarizable model were developed [151]. The inclusion of virtual sites that represent in-plane lone pairs on nitrogen atoms along with anisotropic polarizabilities yielded improved agreement with the QM polarization response as a function orientation as determined using a perturbing ion. The resulting parameters achieved good agreement for pyridine and pyrrole dielectric constants and were validated against additional experimental data such as diffusion constants, heat capacities, and isothermal compressibilities, indicating the ability of the model to be used for the studies of a variety of heterocycles. Extension of the model to nucleic acid bases was subsequently undertaken, though additional optimization of the base parameters was carried out as part of the development of the Drude DNA force field [163–166].

4.6 Sulfur Containing Compounds

Sulfur-containing scaffolds exist in a broad range of pharmaceuticals and natural products [183–185] as well as in many biological systems, such as proteins (e.g. methionine and cysteine). As sulfur atoms are highly polarizable, additive models are significantly limited to simultaneously describe the electronic response of sulfur-containing molecules in both polar and non-polar environments. The polarizable force field for sulfur-containing compounds was derived [153], providing a more accurate representation of chemical groups containing sulfurs, including methanethiol, ethanethiol, propanethiol, ethyl methyl sulfide, and dimethyl disulfide. In parametrizing this model, anisotropic polarizabilities were applied to the sulfur atoms, yielding good agreement with QM water and ion interaction energies as a function of angle or distance. Different polarizability scaling factors were used among the sulfur containing compounds, indicating that the electronic properties of sulfur are sensitive to its chemical environment. A scaling factor of 0.7 was used for thiols to yield good agreement with experimental dielectric constants, while 0.85 was applied to dimethyl disulfide. For ethyl methyl sulfide, which models the parameters used in methionine, a scaling factor of 0.6 was needed to reproduce condensed-phase properties including the dielectric constant and the gas-phase dipole moment. Atom pair-specific LJ parameters [123] between sulfur

6.The π electron system on the aromatic rings results in a negative partial charge in the center of the ring, such that the faces of the benzene ring are able to act as hydrogen bond acceptors [180, 181].

and water oxygen atoms were required to improve the aqueous solvation free energies. The resulting Drude polarizable model demonstrates that the explicit treatment of electronic polarization improves the accuracy of the force field in reproducing experimental properties, such as ΔH_{vap}, V_m, molecular interactions with water, ΔG_{hydr}, as well as dielectric constants, leading to a considerable improvement over the additive model for the same sulfur-containing compounds.

4.7 Ketones and Aldehydes

While ketones and aldehydes are rarely present in drug molecules [186], they are functional groups that occur in acyclic carbohydrates in biological systems. The Drude polarizable force field for aliphatic ketones and aldehydes (e.g. acetaldehyde, propionaldehyde, butaryaldehyde, isobutaryaldehyde, acetone, and butanone) has been developed [155]. The model was then transferred to larger acyclic sugars such as *d*-allose and *d*-psicose. The developed parameters for ketones and aldehydes reproduced properties in good agreement with QM and experimental target data. Notably, the Drude-water interaction energies and distances were in better agreement with the QM data than the additive model, which could be attributed to the lone pairs added on the carbonyl oxygen. The resulting polarizable force field yielded different dipole moments in different environments, with an increase of the dipole moments upon going from the gas phase to pure solvent to aqueous phase consistent with the hydrogen bonding between the monomers in the pure solvent and with water in aqueous solution. Accordingly, it is clear that the treatment of polarization response is important for more accurately simulating systems where molecular species would encounter environments of hydrogen bond interactions or varying polarities.

4.8 Halogenated Ethanes and Benzenes

Halogenated molecules have been widely used in drug development [187, 188], as they have been shown to increase selectivity and binding affinity of inhibitors [189, 190]. Notably, halogens serve as both hydrogen bond acceptors (HBA) [191–195] and as halogen bond (XB) donors [189–191], both of which have been reported to contribute to ligand-protein interactions experimentally [188, 196–200]. The dual roles of halogens result from their anisotropic electron distribution when the halogen (X) is covalently bonded to a carbon atom (C), resulting in the shift of the p_z-orbital on halogens to participate in the formation of the C-X covalent bond. This leads to an electron diminished region on the outer side of the halogen linear to the C-X bond, yielding a slightly positive potential known as a σ-hole [191, 201, 202] which is able to favorably interact with hydrogen bond acceptors (HBA) [189–191, 203]. Simultaneously, the valence electrons on the perpendicular p_x and p_y atomic orbitals of halogens remain occupied yielding an electronegative potential allowing halogens to interact with hydrogen bond donors (HBD) [191]. Such X-HBD interactions have been reported to be more favorable than halogen bonds and of similar strength as canonical hydrogen bonds [204]. Notably, the vdW surface of the halogen becomes asymmetric due to the shifted electron distribution, resulting in a shorter vdW surface on the halogen linear to the C-X covalent bond [205]. Thus, accurate reproduction of XB and X-HBD interactions was emphasized in parametrization to better modeling such important feature in halogens.

The Drude force field was able to reproduce QM molecular dipole moments and polarizabilities, as well as experimental ΔH_{vap}, V_m, ΔG_{hyd}, and dielectric constants for the halogen model compounds [157]. As expected, the halogen polarizable model has the ability to treat the polar character in different environments as shown in Figure 4. The dipole distributions of chlorobenzene (CHLB) and bromobenzene (BROB) from the Drude model both obviously increase from the gas to aqueous phase, whereas the dipole distributions from the additive CGenFF model are nearly the same in the different phases, indicating the lack of polarization response. Similar to other small molecules, the polarizable model was able to reproduce dielectric constants. The halogen polarizable model yielded a significant improvement over the additive model with an average percent difference of only −1% of the experiment results compared to the average percent difference of −33% obtained from the additive halogen model. This improvement of the dielectric constants from the polarizable model is attributed to the explicit treatment of polarizability as previously discussed [44, 145, 206].

One important outcome of the developed halogen model is better treatment of the anisotropic charge distribution and shape of the halogens, which were modeled by inclusion of a virtual particle along the C-X covalent bond, atom pair-specific LJ parameters (NBFIX parameters) on the halogen Drude particle-water hydrogen pairs and on halogen-water oxygen pairs [157]. Notably, the use of the atom pair-specific LJ parameters significantly improved the agreement of the Drude model with the QM interaction energy surfaces for both XB and X-HBD interactions, further indicating its ability to more accurately model the asymmetry of the halogen atoms. Such strategy also resulted in better reproduction of experimental ΔG_{hydr} compared with the additive halogen model in CGenFF [207]. Accordingly, the resulting polarizable force field is expected to be applicable in CADD involving halogenated derivatives as well as simulation studies of halogens in a range of chemical systems.

5. Conclusion

Force fields for small molecules based on additive models have been available for a number of years and shown success in drug design as well as other biochemical and biophysical studies. However, limitation of additive models occur due to the lack of explicit polarization, particularly in cases where polarizable charged groups or atoms, such as ions, are involved which would strongly polarize their coordinating ligands. In addition, the impact of polarization on more accurate treatment of nonpolar moieties such as those in the interior of membranes has been noted. Towards overcoming this limitation, parameters for organic small molecules based on polarizable force fields have started to be developed, dominated by the AMOEBA and Drude models as well as the work of Dang and coworkers [103–105, 208–213]. This chapter focused on the small molecule polarizable force fields based on the classical Drude oscillator model, which utilizes Drude oscillators on non-hydrogen atoms to generate the induced dipole in the context of an intuitive physical picture to model the electronic distribution. In practical aspects, the Drude model has advantages over other polarizable models as the functional forms is similar to those in the additive model, facilitating its implementation in multiple simulation packages, including CHARMM [214–216], NAMD [217, 218], ChemSell QM/MM [219], OpenMM [220] and GROMACS [221].

Currently, the CHARMM Drude polarizable force field for small molecules is still expanding. For example, the development of parameters for halogen-containing molecules greatly expands the range of chemical space covered by the Drude force field relevant to medicinal compounds [157]. Similarly to the CGenFF force field [13] that is a part of the CHARMM all-atom additive biological force field, efforts are ongoing towards development of a Drude General Force Field (DGenFF) that will cover a wide range of chemical groups in drug-like molecules. In the end, the polarizable force field for these molecules will be applicable in chemical and biophysical studies as well as be able to be useful for ligands in the study of computer-aided drug design.

Acknowledgements

This work was supported by National Institutes of Health grants GM051501, GM070855 and GM072558. The University of Maryland Computer-Aided Drug Design Center and XSEDE are acknowledged for their generous allocations of computer time.

References

1. Durrant JD, McCammon JA (2011) Molecular dynamics simulations and drug discovery. BMC Biol 9:71 [PubMed: 22035460]
2. Bernard D, Coop A, MacKerell AD Jr (2003) 2D Conformationally Sampled Pharmacophore: A Ligand-Based Pharmacophore To Differentiate δ Opioid Agonists from Antagonists. J Am Chem Soc 125:3101–3107 [PubMed: 12617677]
3. Bernard D, Coop A, MacKerell AD Jr (2005) Conformationally Sampled Pharmacophore for Peptidic δ Opioid Ligands. J Med Chem 48:7773–7780 [PubMed: 16302816]
4. Bernard D, Coop A, MacKerell AD Jr (2007) Quantitative Conformationally Sampled Pharmacophore for δ Opioid Ligands: Reevaluation of Hydrophobic Moieties Essential for Biological Activity. J Med Chem 50:1799–1809 [PubMed: 17367120]
5. Shim J, MacKerell AD Jr (2011) Computational ligand-based rational design: role of conformational sampling and force fields in model development. MedChemComm 2:356–370 [PubMed: 21716805]
6. Shim J, Coop A, MacKerell AD Jr (2011) Consensus 3D Model of μ-Opioid Receptor Ligand Efficacy Based on a Quantitative Conformationally Sampled Pharmacophore. J Phys Chem B 115:7487–7496 [PubMed: 21563754]
7. Kuntz ID (1992) Structure-Based Strategies for Drug Design and Discovery. Science 257:1078–1082 [PubMed: 1509259]
8. Anderson AC (2003) The Process of Structure-Based Drug Design. Chem Biol 10:787–797 [PubMed: 14522049]
9. Sliwoski G, Kothiwale S, Meiler J, Lowe EW (2014) Computational Methods in Drug Discovery. Pharmacol Rev 66:334–395 [PubMed: 24381236]
10. De Vivo M, Masetti M, Bottegoni G, Cavalli A (2016) Role of Molecular Dynamics and Related Methods in Drug Discovery. J Med Chem 59:4035–4061 [PubMed: 26807648]
11. Jorgensen WL, Maxwell DS, Tirado-Rives J (1996) Development and Testing of the OPLS All-Atom Force Field on Conformational Energetics and Properties of Organic Liquids. J Am Chem Soc 118:11225–11236
12. Harder E, Damm W, Maple J, et al. (2016) OPLS3: A Force Field Providing Broad Coverage of Drug-like Small Molecules and Proteins. J Chem Theory Comput 12:281–296 [PubMed: 26584231]
13. Vanommeslaeghe K, Hatcher E, Acharya C, et al. (2010) CHARMM General Force Field (CGenFF): A force field for drug-like molecules compatible with the CHARMM all-atom additive biological force fields. J Comput Chem 31:671–690 [PubMed: 19575467]

14. Vanommeslaeghe K, MacKerell AD Jr (2012) Automation of the CHARMM General Force Field (CGenFF) I: Bond Perception and Atom Typing. J Chem Inf Model 52:3144–3154 [PubMed: 23146088]
15. Vanommeslaeghe K, Raman EP, MacKerell AD Jr (2012) Automation of the CHARMM General Force Field (CGenFF) II: Assignment of Bonded Parameters and Partial Atomic Charges. J Chem Inf Model 52:3155–3168
16. Yu W, He X, Vanommeslaeghe K, MacKerell AD Jr (2012) Extension of the CHARMM General Force Field to sulfonyl-containing compounds and its utility in biomolecular simulations. J Comput Chem 33:2451–2468 [PubMed: 22821581]
17. Wang J, Wolf RM, Caldwell JW, Kollman PA, Case DA (2004) Development and testing of a general amber force field. J Comput Chem 25:1157–1174 [PubMed: 15116359]
18. Wang J, Wang W, Kollman PA, Case DA (2006) Automatic atom type and bond type perception in molecular mechanical calculations. J Mol Graph Model 25:247–260 [PubMed: 16458552]
19. Halgren TA (1996) Merck molecular force field. I. Basis, form, scope, parameterization, and performance of MMFF94. J Comput Chem 17:490–519
20. Halgren TA (1996) Merck molecular force field. II. MMFF94 van der Waals and electrostatic parameters for intermolecular interactions. J Comput Chem 17:520–552
21. Halgren TA (1996) Merck molecular force field. III. Molecular geometries and vibrational frequencies for MMFF94. J Comput Chem 17:553–586
22. Halgren TA, Nachbar RB (1996) Merck molecular force field. IV. conformational energies and geometries for MMFF94. J Comput Chem 17:587–615
23. Halgren TA (1996) Merck molecular force field. V. Extension of MMFF94 using experimental data, additional computational data, and empirical rules. J Comput Chem 17:616–641
24. Daura X, Mark AE, Van Gunsteren WF (1998) Parametrization of aliphatic CHn united atoms of GROMOS96 force field. J Comput Chem 19:535–547
25. Schuler LD, Daura X, van Gunsteren WF (2001) An improved GROMOS96 force field for aliphatic hydrocarbons in the condensed phase. J Comput Chem 22:1205–1218
26. Oostenbrink C, Villa A, Mark AE, Van Gunsteren WF (2004) A biomolecular force field based on the free enthalpy of hydration and solvation: The GROMOS force-field parameter sets 53A5 and 53A6. J Comput Chem 25:1656–1676 [PubMed: 15264259]
27. Horta BAC, Fuchs PFJ, van Gunsteren WF, Hünenberger PH (2011) New Interaction Parameters for Oxygen Compounds in the GROMOS Force Field: Improved Pure-Liquid and Solvation Properties for Alcohols, Ethers, Aldehydes, Ketones, Carboxylic Acids, and Esters. J Chem Theory Comput 7:1016–1031 [PubMed: 26606351]
28. Horta BAC, Merz PT, Fuchs PFJ, Dolenc J, Riniker S, Hünenberger PH (2016) A GROMOS-Compatible Force Field for Small Organic Molecules in the Condensed Phase: The 2016H66 Parameter Set. J Chem Theory Comput 12:3825–3850 [PubMed: 27248705]
29. Malde AK, Zuo L, Breeze M, Stroet M, Poger D, Nair PC, Oostenbrink C, Mark AE (2011) An Automated Force Field Topology Builder (ATB) and Repository: Version 1.0. J Chem Theory Comput 7:4026–4037 [PubMed: 26598349]
30. Aalten DMF van, Bywater R, Findlay JBC, Hendlich M, Hooft RWW, Vriend G (1996) PRODRG, a program for generating molecular topologies and unique molecular descriptors from coordinates of small molecules. J Comput Aided Mol Des 10:255–262 [PubMed: 8808741]
31. Schüttelkopf AW, van Aalten DMF (2004) PRODRG: a tool for high-throughput crystallography of protein-ligand complexes. Acta Crystallogr D Biol Crystallogr 60:1355–1363 [PubMed: 15272157]
32. Yesselman JD, Price DJ, Knight JL, Brooks CL (2012) MATCH: an atom-typing toolset for molecular mechanics force fields. J Comput Chem 33:189–202 [PubMed: 22042689]
33. Zoete V, Cuendet MA, Grosdidier A, Michielin O (2011) SwissParam: a fast force field generation tool for small organic molecules. J Comput Chem 32:2359–2368 [PubMed: 21541964]
34. Vanommeslaeghe K, MacKerell AD Jr (2015) CHARMM additive and polarizable force fields for biophysics and computer-aided drug design. Biochim Biophys Acta BBA - Gen Subj 1850:861–871

35. MacKerell AD Jr (2004) Empirical force fields for biological macromolecules: overview and issues. J Comput Chem 25:1584–1604 [PubMed: 15264253]
36. Lide DR (2008) CRC handbook of chemistry and physics. [electronic resource] Boca Raton, Fla. : CRC Press ; Taylor & Francis, c2009.
37. Gregory JK, Clary DC, Liu K, Brown MG, Saykally RJ (1997) The Water Dipole Moment in Water Clusters. Science 275:814–817 [PubMed: 9012344]
38. Badyal YS, Saboungi M-L, Price DL, Shastri SD, Haeffner DR, Soper AK (2000) Electron distribution in water. J Chem Phys 112:9206–9208
39. Huang J, Lopes PEM, Roux B, MacKerell AD Jr (2014) Recent Advances in Polarizable Force Fields for Macromolecules: Microsecond Simulations of Proteins Using the Classical Drude Oscillator Model. J Phys Chem Lett 5:3144–3150 [PubMed: 25247054]
40. Lopes PEM, Guvench O, MacKerell AD Jr (2015) Current Status of Protein Force Fields for Molecular Dynamics. Methods Mol Biol Clifton NJ 1215:47–71
41. Shi Y, Ren P, Schnieders M, Piquemal J-P (2015) Polarizable Force Fields for Biomolecular Modeling. In: Parrill AL, Lipkowitz KB (eds) Rev. Comput. Chem Vol. 28 John Wiley & Sons, Inc, pp 51–86
42. Xu P, Wang J, Xu Y, et al. (2015) Advancement of Polarizable Force Field and Its Use for Molecular Modeling and Design. In: Adv. Struct. Bioinforma Springer, Dordrecht, pp 19–32
43. Baker CM (2015) Polarizable force fields for molecular dynamics simulations of biomolecules. Wiley Interdiscip Rev Comput Mol Sci 5:241–254
44. Lemkul JA, Huang J, Roux B, MacKerell AD Jr (2016) An Empirical Polarizable Force Field Based on the Classical Drude Oscillator Model: Development History and Recent Applications. Chem Rev 116:4983–5013 [PubMed: 26815602]
45. Archontis G, Leontidis E, Andreou G (2005) Attraction of Iodide Ions by the Free Water Surface, Revealed by Simulations with a Polarizable Force Field Based on Drude Oscillators. J Phys Chem B 109:17957–17966 [PubMed: 16853305]
46. Jungwirth P, Tobias DJ (2006) Specific Ion Effects at the Air/Water Interface. Chem Rev 106:1259–1281 [PubMed: 16608180]
47. Yu H, Whitfield TW, Harder E, Lamoureux G, Vorobyov I, Anisimov VM, MacKerell AD Jr, Roux B (2010) Simulating Monovalent and Divalent Ions in Aqueous Solution Using a Drude Polarizable Force Field. J Chem Theory Comput 6:774–786 [PubMed: 20300554]
48. Bauer BA, Ou S, Patel S (2012) Solvation Structure and Energetics of Single Ions at the Aqueous Liquid-Vapor Interface. Chem Phys Lett 527:22–26 [PubMed: 23136448]
49. Allen TW, Andersen OS, Roux B (2004) Energetics of ion conduction through the gramicidin channel. Proc Natl Acad Sci U S A 101:117–122 [PubMed: 14691245]
50. Allen TW, Andersen OS, Roux B (2006) Molecular dynamics — potential of mean force calculations as a tool for understanding ion permeation and selectivity in narrow channels. Biophys Chem 124:251–267 [PubMed: 16781050]
51. Patel S, Davis JE, Bauer BA (2009) Exploring Ion Permeation Energetics in Gramicidin A Using Polarizable Charge Equilibration Force Fields. J Am Chem Soc 131:13890 [PubMed: 19788320]
52. Harder E, MacKerell AD Jr, Roux B (2009) Many-Body Polarization Effects and the Membrane Dipole Potential. J Am Chem Soc 131:2760–2761 [PubMed: 19199514]
53. Bauer BA, Lucas TR, Meninger DJ, Patel S (2011) Water Permeation Through DMPC Lipid Bilayers using Polarizable Charge Equilibration Force Fields. Chem Phys Lett 508:289–294 [PubMed: 21647243]
54. Soto P, Mark AE (2002) The Effect of the Neglect of Electronic Polarization in Peptide Folding Simulations. J Phys Chem B 106:12830–12833
55. Jiao D, Golubkov PA, Darden TA, Ren P (2008) Calculation of protein–ligand binding free energy by using a polarizable potential. Proc Natl Acad Sci 105:6290–6295 [PubMed: 18427113]
56. Jiao D, Zhang J, Duke RE, Li G, Schnieders MJ, Ren P (2009) Trypsin-ligand binding free energies from explicit and implicit solvent simulations with polarizable potential. J Comput Chem 30:1701–1711 [PubMed: 19399779]

57. Shi Y, Zhu CZ, Martin SF, Ren P (2012) Probing the Effect of Conformational Constraint on Phosphorylated Ligand Binding to an SH2 Domain using Polarizable Force Field Simulations. J Phys Chem B 116:1716–1727 [PubMed: 22214214]
58. Zhang J, Shi Y, Ren P (2012) Polarizable Force Fields for Scoring Protein–Ligand Interactions. In: Gohlke H (ed) Protein-Ligand Interact Wiley-VCH Verlag GmbH & Co. KGaA, pp 99–120
59. de Courcy B, Piquemal J-P, Garbay C, Gresh N (2010) Polarizable water molecules in ligand-macromolecule recognition. Impact on the relative affinities of competing pyrrolopyrimidine inhibitors for FAK kinase. J Am Chem Soc 132:3312–3320 [PubMed: 20178314]
60. Gresh N, de Courcy B, Piquemal J-P, Foret J, Courtiol-Legourd S, Salmon L (2011) Polarizable water networks in ligand-metalloprotein recognition. Impact on the relative complexation energies of Zn-dependent phosphomannose isomerase with D-mannose 6-phosphate surrogates. J Phys Chem B 115:8304–8316 [PubMed: 21650197]
61. Best RB, Zhu X, Shim J, Lopes PEM, Mittal J, Feig M, MacKerell AD Jr (2012) Optimization of the additive CHARMM all-atom protein force field targeting improved sampling of the backbone φ, ψ and side-chain χ1 and χ2 dihedral angles. J Chem Theory Comput 8:3257–3273 [PubMed: 23341755]
62. MacKerell AD Jr, Banavali NK (2000) All-atom empirical force field for nucleic acids: II. Application to molecular dynamics simulations of DNA and RNA in solution. J Comput Chem 21:105–120
63. Foloppe N, MacKerell AD Jr (2000) All-atom empirical force field for nucleic acids: I. Parameter optimization based on small molecule and condensed phase macromolecular target data. J Comput Chem 21:86–104
64. Denning EJ, Priyakumar UD, Nilsson L, MacKerell AD Jr (2011) Impact of 2'-hydroxyl sampling on the conformational properties of RNA: update of the CHARMM all-atom additive force field for RNA. J Comput Chem 32:1929–1943 [PubMed: 21469161]
65. Hart K, Foloppe N, Baker CM, Denning EJ, Nilsson L, MacKerell AD Jr (2012) Optimization of the CHARMM additive force field for DNA: Improved treatment of the BI/BII conformational equilibrium. J Chem Theory Comput 8:348–362 [PubMed: 22368531]
66. Feller SE, Gawrisch K, MacKerell AD Jr (2002) Polyunsaturated fatty acids in lipid bilayers: intrinsic and environmental contributions to their unique physical properties. J Am Chem Soc 124:318–326 [PubMed: 11782184]
67. Klauda JB, Venable RM, Freites JA, O'Connor JW, Tobias DJ, Mondragon-Ramirez C, Vorobyov I, MacKerell AD Jr, Pastor RW (2010) Update of the CHARMM All-Atom Additive Force Field for Lipids: Validation on Six Lipid Types. J Phys Chem B 114:7830–7843 [PubMed: 20496934]
68. Guvench O, Hatcher E, Venable RM, Pastor RW, MacKerell AD Jr (2009) CHARMM Additive All-Atom Force Field for Glycosidic Linkages between Hexopyranoses. J Chem Theory Comput 5:2353–2370 [PubMed: 20161005]
69. Guvench O, Mallajosyula SS, Raman EP, Hatcher E, Vanommeslaeghe K, Foster TJ, Jamison FW, MacKerell AD Jr (2011) CHARMM additive all-atom force field for carbohydrate derivatives and its utility in polysaccharide and carbohydrate-protein modeling. J Chem Theory Comput 7:3162–3180 [PubMed: 22125473]
70. Klauda JB, Monje V, Kim T, Im W (2012) Improving the CHARMM Force Field for Polyunsaturated Fatty Acid Chains. J Phys Chem B 116:9424–9431 [PubMed: 22697583]
71. Guvench O, Greene SN, Kamath G, Brady JW, Venable RM, Pastor RW, MacKerell AD Jr (2008) Additive empirical force field for hexopyranose monosaccharides. J Comput Chem 29:2543–2564 [PubMed: 18470966]
72. Hatcher E, Guvench O, MacKerell AD Jr (2009) CHARMM Additive All-Atom Force Field for Acyclic Polyalcohols, Acyclic Carbohydrates and Inositol. J Chem Theory Comput 5:1315–1327 [PubMed: 20160980]
73. Hatcher E, Guvench O, MacKerell AD Jr (2009) CHARMM Additive All-Atom Force Field for Aldopentofuranoses, Methyl-aldopentofuranosides, and Fructofuranose. J Phys Chem B 113:12466–12476 [PubMed: 19694450]

74. Raman EP, Guvench O, MacKerell AD Jr (2010) CHARMM Additive All-Atom Force Field for Glycosidic Linkages in Carbohydrates Involving Furanoses. J Phys Chem B 114:12981–12994 [PubMed: 20845956]

75. Mallajosyula SS, MacKerell AD Jr (2011) Influence of Solvent and Intramolecular Hydrogen Bonding on the Conformational Properties of O-Linked Glycopeptides. J Phys Chem B 115:11215–11229 [PubMed: 21823626]

76. Mallajosyula SS, Guvench O, Hatcher E, MacKerell AD Jr (2012) CHARMM Additive All-Atom Force Field for Phosphate and Sulfate Linked to Carbohydrates. J Chem Theory Comput 8:759–776 [PubMed: 22685386]

77. Mayne CG, Saam J, Schulten K, Tajkhorshid E, Gumbart JC (2013) Rapid parameterization of small molecules using the force field toolkit. J Comput Chem 34:2757–2770 [PubMed: 24000174]

78. Huang L, Roux B (2013) Automated Force Field Parameterization for Nonpolarizable and Polarizable Atomic Models Based on Ab Initio Target Data. J Chem Theory Comput 9:3543–3556

79. Ross WS, Hardin CC (1994) Ion-Induced Stabilization of the G-DNA Quadruplex: Free Energy Perturbation Studies. J Am Chem Soc 116:6070–6080

80. Cornell WD, Cieplak P, Bayly CI, Gould IR, Merz KM, Ferguson DM, Spellmeyer DC, Fox T, Caldwell JW, Kollman PA (1996) A Second Generation Force Field for the Simulation of Proteins, Nucleic Acids, and Organic Molecules J. Am. Chem. Soc. 1995, 117, 5179–5197. J Am Chem Soc 118:2309–2309

81. Ha SN, Giammona A, Field M, Brady JW (1988) A revised potential-energy surface for molecular mechanics studies of carbohydrates. Carbohydr Res 180:207–221 [PubMed: 3203342]

82. Homans SW (1990) A molecular mechanical force field for the conformational analysis of oligosaccharides: comparison of theoretical and crystal structures of Man alpha 1–3Man beta 1–4GlcNAc. Biochemistry (Mosc) 29:9110–9118 [PubMed: 2271581]

83. Kirschner KN, Yongye AB, Tschampel SM, González-Outeiriño J, Daniels CR, Foley BL, Woods RJ (2008) GLYCAM06: a generalizable biomolecular force field. Carbohydrates. J Comput Chem 29:622–655 [PubMed: 17849372]

84. Dickson CJ, Madej BD, Skjevik ÅA, Betz RM, Teigen K, Gould IR, Walker RC (2014) Lipid14: The Amber Lipid Force Field. J Chem Theory Comput 10:865–879 [PubMed: 24803855]

85. Bayly CI, Cieplak P, Cornell W, Kollman PA (1993) A well-behaved electrostatic potential based method using charge restraints for deriving atomic charges: the RESP model. J Phys Chem 97:10269–10280

86. Cieplak P, Cornell WD, Bayly C, Kollman PA (1995) Application of the multimolecule and multiconformational RESP methodology to biopolymers: Charge derivation for DNA, RNA, and proteins. J Comput Chem 16:1357–1377

87. Jakalian A, Jack DB, Bayly CI (2002) Fast, efficient generation of high-quality atomic charges. AM1-BCC model: II. Parameterization and validation. J Comput Chem 23:1623–1641 [PubMed: 12395429]

88. Rappe AK, Casewit CJ, Colwell KS, Goddard WA, Skiff WM (1992) UFF, a full periodic table force field for molecular mechanics and molecular dynamics simulations. J Am Chem Soc 114:10024–10035

89. Rick SW, Stuart SJ, Berne BJ (1994) Dynamical fluctuating charge force fields: Application to liquid water. J Chem Phys 101:6141–6156

90. Rick SW, Berne BJ (1996) Dynamical Fluctuating Charge Force Fields: The Aqueous Solvation of Amides. J Am Chem Soc 118:672–679

91. Stern HA, Rittner F, Berne BJ, Friesner RA (2001) Combined fluctuating charge and polarizable dipole models: Application to a five-site water potential function. J Chem Phys 115:2237–2251

92. Patel S, Brooks CL III (2004) CHARMM fluctuating charge force field for proteins: I parameterization and application to bulk organic liquid simulations. J Comput Chem 25:1–16 [PubMed: 14634989]

93. Patel S, MacKerell AD Jr, Brooks CL (2004) CHARMM fluctuating charge force field for proteins: II Protein/solvent properties from molecular dynamics simulations using a nonadditive electrostatic model. J Comput Chem 25:1504–1514 [PubMed: 15224394]

94. Stuart SJ, Berne BJ (1996) Effects of Polarizability on the Hydration of the Chloride Ion. J Phys Chem 100:11934–11943
95. Kaminski GA, Stern HA, Berne BJ, Friesner RA, Cao YX, Murphy RB, Zhou R, Halgren TA (2002) Development of a polarizable force field for proteins via ab initio quantum chemistry: first generation model and gas phase tests. J Comput Chem 23:1515–1531 [PubMed: 12395421]
96. Dang LX, Rice JE, Caldwell J, Kollman PA (1991) Ion solvation in polarizable water: molecular dynamics simulations. J Am Chem Soc 113:2481–2486
97. Caldwell JW, Kollman PA (1995) Structure and Properties of Neat Liquids Using Nonadditive Molecular Dynamics: Water, Methanol, and N-Methylacetamide. J Phys Chem 99:6208–6219
98. Caldwell JW, Kollman PA (1995) Cation-.pi. Interactions: Nonadditive Effects Are Critical in Their Accurate Representation. J Am Chem Soc 117:4177–4178
99. Cieplak P, Caldwell J, Kollman P (2001) Molecular mechanical models for organic and biological systems going beyond the atom centered two body additive approximation: aqueous solution free energies of methanol and N-methyl acetamide, nucleic acid base, and amide hydrogen bonding and chloroform/water partition coefficients of the nucleic acid bases. J Comput Chem 22:1048–1057
100. Wang Z-X, Zhang W, Wu C, Lei H, Cieplak P, Duan Y (2006) Strike a Balance: Optimization of Backbone Torsion Parameters of AMBER Polarizable Force Field for Simulations of Proteins and Peptides. J Comput Chem 27:781–790 [PubMed: 16526038]
101. Xie W, Pu J, MacKerell AD Jr, Gao J (2007) Development of a polarizable intermolecular potential function (PIPF) for liquid amides and alkanes. J Chem Theory Comput 3:1878–1889 [PubMed: 18958290]
102. Liu Y-P, Kim K, Berne BJ, Friesner RA, Rick SW (1998) Constructing ab initio force fields for molecular dynamics simulations. J Chem Phys 108:4739–4755
103. Dang LX, Chang T-M (1997) Molecular dynamics study of water clusters, liquid, and liquid–vapor interface of water with many-body potentials. J Chem Phys 106:8149–8159
104. Sun X, Wick CD, Dang LX (2011) Computational Study of Ion Distributions at the Air/Liquid Methanol Interface. J Phys Chem A 115:5767–5773 [PubMed: 20939498]
105. Chang T-M, Dang LX (2014) Computational Studies of [bmim][PF6]/n-Alcohol Interfaces with Many-Body Potentials. J Phys Chem A 118:7186–7193 [PubMed: 24063438]
106. Wang J, Cieplak P, Li J, Hou T, Luo R, Duan Y (2011) Development of Polarizable Models for Molecular Mechanical Calculations I: Parameterization of Atomic Polarizability. J Phys Chem B 115:3091–3099 [PubMed: 21391553]
107. Wang J, Cieplak P, Li J, Wang J, Cai Q, Hsieh M, Lei H, Luo R, Duan Y (2011) Development of Polarizable Models for Molecular Mechanical Calculations II: Induced Dipole Models Significantly Improve Accuracy of Intermolecular Interaction Energies. J Phys Chem B 115:3100–3111 [PubMed: 21391583]
108. Wang J, Cieplak P, Cai Q, Hsieh M-J, Wang J, Duan Y, Luo R (2012) Development of Polarizable Models for Molecular Mechanical Calculations. 3. Polarizable Water Models Conforming to Thole Polarization Screening Schemes. J Phys Chem B 116:7999–8008 [PubMed: 22712654]
109. Wang J, Cieplak P, Li J, Cai Q, Hsieh M-J, Luo R, Duan Y (2012) Development of Polarizable Models for Molecular Mechanical Calculations. 4. van der Waals Parametrization. J Phys Chem B 116:7088–7101 [PubMed: 22612331]
110. Ren P, Ponder JW (2003) Polarizable Atomic Multipole Water Model for Molecular Mechanics Simulation. J Phys Chem B 107:5933–5947
111. Ponder JW, Wu C, Ren P, et al. (2010) Current Status of the AMOEBA Polarizable Force Field. J Phys Chem B 114:2549–2564 [PubMed: 20136072]
112. Shi Y, Xia Z, Zhang J, Best R, Wu C, Ponder JW, Ren P (2013) Polarizable Atomic Multipole-Based AMOEBA Force Field for Proteins. J Chem Theory Comput 9:4046–4063 [PubMed: 24163642]
113. Wang L-P, Head-Gordon T, Ponder JW, Ren P, Chodera JD, Eastman PK, Martinez TJ, Pande VS (2013) Systematic Improvement of a Classical Molecular Model of Water. J Phys Chem B 117:9956–9972 [PubMed: 23750713]
114. Albaugh A, Niklasson AMN, Head-Gordon T (2017) Accurate Classical Polarization Solution with No Self-Consistent Field Iterations. J Phys Chem Lett 8:1714–1723 [PubMed: 28350167]

115. Albaugh A, Demerdash O, Head-Gordon T (2015) An efficient and stable hybrid extended Lagrangian/self-consistent field scheme for solving classical mutual induction. J Chem Phys 143:174104 [PubMed: 26547155]
116. Simmonett AC, Pickard FC, Ponder JW, Brooks BR (2016) An empirical extrapolation scheme for efficient treatment of induced dipoles. J Chem Phys doi: 10.1063/1.4964866
117. Simmonett AC, Pickard FC, Schaefer HF, Brooks BR (2014) An efficient algorithm for multipole energies and derivatives based on spherical harmonics and extensions to particle mesh Ewald. J Chem Phys 140:184101 [PubMed: 24832247]
118. Huang J, Simmonett AC, Pickard FC, MacKerell AD Jr, Brooks BR (2017) Mapping the Drude polarizable force field onto a multipole and induced dipole model. J Chem Phys 147:161702 [PubMed: 29096511]
119. Harder E, Anisimov VM, Whitfield T, MacKerell AD Jr, Roux B (2008) Understanding the Dielectric Properties of Liquid Amides from a Polarizable Force Field. J Phys Chem B 112:3509–3521 [PubMed: 18302362]
120. Harder E, Anisimov VM, Vorobyov IV, Lopes PEM, Noskov SY, MacKerell AD Jr, Roux B (2006) Atomic Level Anisotropy in the Electrostatic Modeling of Lone Pairs for a Polarizable Force Field Based on the Classical Drude Oscillator. J Chem Theory Comput 2:1587–1597 [PubMed: 26627029]
121. Thole BT (1981) Molecular polarizabilities calculated with a modified dipole interaction. Chem Phys 59:341–350
122. Allen MP, Tildesley DJ (2017) Computer Simulation of Liquids, Second Edition, New to this Edition: Oxford University Press, Oxford, New York
123. Baker CM, Lopes PEM, Zhu X, Roux B, MacKerell AD Jr (2010) Accurate Calculation of Hydration Free Energies using Pair-Specific Lennard-Jones Parameters in the CHARMM Drude Polarizable Force Field. J Chem Theory Comput 6:1181–1198 [PubMed: 20401166]
124. Chowdhary J, Harder E, Lopes PEM, Huang L, MacKerell AD Jr, Roux B (2013) A Polarizable Force Field of Dipalmitoylphosphatidylcholine Based on the Classical Drude Model for Molecular Dynamics Simulations of Lipids. J Phys Chem B 117:9142–9160 [PubMed: 23841725]
125. Kunz A-PE, van Gunsteren WF (2009) Development of a nonlinear classical polarization model for liquid water and aqueous solutions: COS/D. J Phys Chem A 113:11570–11579 [PubMed: 19663490]
126. Lamoureux G, Roux B (2003) Modeling induced polarization with classical Drude oscillators: Theory and molecular dynamics simulation algorithm. J Chem Phys 119:3025–3039
127. Lucas TR, Bauer BA, Patel S (2012) Charge equilibration force fields for molecular dynamics simulations of lipids, bilayers, and integral membrane protein systems. Biochim Biophys Acta BBA - Biomembr 1818:318–329
128. Zhong Y, Bauer BA, Patel S (2011) Solvation properties of N-acetyl-β-glucosamine: molecular dynamics study incorporating electrostatic polarization. J Comput Chem 32:3339–3353 [PubMed: 21898464]
129. Zhong Y, Patel S (2013) Binding structures of tri-N-acetyl-β-glucosamine in hen egg white lysozyme using molecular dynamics with a polarizable force field. J Comput Chem 34:163–174 [PubMed: 23109228]
130. Ou S, Patel S (2013) Temperature dependence and energetics of single ions at the aqueous liquid-vapor interface. J Phys Chem B 117:6512–6523 [PubMed: 23537166]
131. Hu Y, Ou S, Patel S (2013) Free energetics of arginine permeation into model DMPC lipid bilayers: coupling of effective counterion concentration and lateral bilayer dimensions. J Phys Chem B 117:11641–11653 [PubMed: 23888915]
132. Grossfield A, Ren P, Ponder JW (2003) Ion solvation thermodynamics from simulation with a polarizable force field. J Am Chem Soc 125:15671–15682 [PubMed: 14664617]
133. Wu JC, Piquemal J-P, Chaudret R, Reinhardt P, Ren P (2010) Polarizable molecular dynamics simulation of Zn(II) in water using the AMOEBA force field. J Chem Theory Comput 6:2059–2070 [PubMed: 21116445]

134. Ponder JW, Richards FM (1987) An efficient newton-like method for molecular mechanics energy minimization of large molecules. J Comput Chem 8:1016–1024
135. Ren P, Wu C, Ponder JW (2011) Polarizable Atomic Multipole-Based Molecular Mechanics for Organic Molecules. J Chem Theory Comput 7:3143–3161 [PubMed: 22022236]
136. Mu X, Wang Q, Wang L-P, Fried SD, Piquemal J-P, Dalby KN, Ren P (2014) Modeling Organochlorine Compounds and the σ-Hole Effect Using a Polarizable Multipole Force Field. J Phys Chem B 118:6456–6465 [PubMed: 24484473]
137. Ren P, Ponder JW (2004) Temperature and Pressure Dependence of the AMOEBA Water Model. J Phys Chem B 108:13427–13437
138. Piquemal J-P, Perera L, Cisneros GA, Ren P, Pedersen LG, Darden TA (2006) Towards accurate solvation dynamics of divalent cations in water using the polarizable amoeba force field: From energetics to structure. J Chem Phys 125:054511 [PubMed: 16942230]
139. Schnieders MJ, Fenn TD, Pande VS, Brunger AT (2009) Polarizable atomic multipole X-ray refinement: application to peptide crystals. Acta Crystallogr D Biol Crystallogr 65:952–965 [PubMed: 19690373]
140. Zhang J, Yang W, Piquemal J-P, Ren P (2012) Modeling Structural Coordination and Ligand Binding in Zinc Proteins with a Polarizable Potential. J Chem Theory Comput 8:1314–1324 [PubMed: 22754403]
141. Ren P, Ponder JW (2002) Consistent treatment of inter- and intramolecular polarization in molecular mechanics calculations. J Comput Chem 23:1497–1506 [PubMed: 12395419]
142. Shi Y, Jiao D, Schnieders MJ, Ren P (2009) Trypsin-ligand binding free energy calculation with AMOEBA. Conf Proc Annu Int Conf IEEE Eng Med Biol Soc IEEE Eng Med Biol Soc Annu Conf 2009:2328–2331
143. Lamoureux G, Harder E, Vorobyov IV, Roux B, MacKerell AD Jr (2006) A polarizable model of water for molecular dynamics simulations of biomolecules. Chem Phys Lett 418:245–249
144. Yu W, Lopes PEM, Roux B, MacKerell AD Jr (2013) Six-site polarizable model of water based on the classical Drude oscillator. J Chem Phys doi: 10.1063/1.4774577
145. Vorobyov IV, Anisimov VM, MacKerell AD Jr (2005) Polarizable Empirical Force Field for Alkanes Based on the Classical Drude Oscillator Model. J Phys Chem B 109:18988–18999 [PubMed: 16853445]
146. Noskov SY, Lamoureux G, Roux B (2005) Molecular Dynamics Study of Hydration in Ethanol −Water Mixtures Using a Polarizable Force Field. J Phys Chem B 109:6705–6713 [PubMed: 16851754]
147. Anisimov VM, Lamoureux G, Vorobyov IV, Huang N, Roux B, MacKerell AD Jr (2005) Determination of Electrostatic Parameters for a Polarizable Force Field Based on the Classical Drude Oscillator. J Chem Theory Comput 1:153–168 [PubMed: 26641126]
148. Lopes PEM, Lamoureux G, Roux B, MacKerell AD Jr (2007) Polarizable Empirical Force Field for Aromatic Compounds Based on the Classical Drude Oscillator. J Phys Chem B 111:2873–2885 [PubMed: 17388420]
149. Anisimov VM, Vorobyov IV, Roux B, MacKerell AD Jr (2007) Polarizable empirical force field for the primary and secondary alcohol series based on the classical Drude model. J Chem Theory Comput 3:1927 [PubMed: 18802495]
150. Vorobyov I, Anisimov VM, Greene S, Venable RM, Moser A, Pastor RW, MacKerell AD Jr (2007) Additive and Classical Drude Polarizable Force Fields for Linear and Cyclic Ethers. J Chem Theory Comput 3:1120–1133 [PubMed: 26627431]
151. Lopes PEM, Lamoureux G, MacKerell AD Jr (2009) Polarizable empirical force field for nitrogen-containing heteroaromatic compounds based on the classical Drude oscillator. J Comput Chem 30:1821–1838 [PubMed: 19090564]
152. Baker CM, MacKerell AD Jr (2010) Polarizability rescaling and atom-based Thole scaling in the CHARMM Drude polarizable force field for ethers. J Mol Model 16:567–576 [PubMed: 19705172]
153. Zhu X, MacKerell AD Jr (2010) Polarizable empirical force field for sulfur-containing compounds based on the classical Drude oscillator model. J Comput Chem 31:2330–2341 [PubMed: 20575015]

154. Lin B, Lopes PEM, Roux B, MacKerell AD Jr (2013) Kirkwood-Buff analysis of aqueous N-methylacetamide and acetamide solutions modeled by the CHARMM additive and Drude polarizable force fields. J Chem Phys 139:084509 [PubMed: 24007020]

155. Small MC, Aytenfisu AH, Lin F-Y, He X, MacKerell AD Jr (2017) Drude polarizable force field for aliphatic ketones and aldehydes, and their associated acyclic carbohydrates. J Comput Aided Mol Des 31:349–363 [PubMed: 28190218]

156. Lin F-Y, Lopes PEM, Harder E, Roux B, MacKerell AD (2018) Polarizable Force Field for Molecular Ions Based on the Classical Drude Oscillator. J Chem Inf Model 58:993–1004 [PubMed: 29624370]

157. Lin F-Y, MacKerell AD (2018) Polarizable Empirical Force Field for Halogen-Containing Compounds Based on the Classical Drude Oscillator. J Chem Theory Comput 14:1083–1098 [PubMed: 29357257]

158. He X, Lopes PEM, MacKerell AD Jr (2013) Polarizable Empirical Force Field for Acyclic Polyalcohols Based on the Classical Drude Oscillator. Biopolymers 99:724–738 [PubMed: 23703219]

159. Patel DS, He X, MacKerell AD Jr (2015) Polarizable Empirical Force Field for Hexopyranose Monosaccharides Based on the Classical Drude Oscillator. J Phys Chem B 119:637–652 [PubMed: 24564643]

160. Jana M, MacKerell AD Jr (2015) CHARMM Drude Polarizable Force Field for Aldopentofuranoses and Methyl-aldopentofuranosides. J Phys Chem B 119:7846–7859 [PubMed: 26018564]

161. Yang M, Aytenfisu AH, MacKerell AD (2018) Proper balance of solvent-solute and solute-solute interactions in the treatment of the diffusion of glucose using the Drude polarizable force field. Carbohydr Res 457:41–50 [PubMed: 29422120]

162. Lopes PEM, Huang J, Shim J, Luo Y, Li H, Roux B, MacKerell AD Jr (2013) Force Field for Peptides and Proteins based on the Classical Drude Oscillator. J Chem Theory Comput 9:5430–5449 [PubMed: 24459460]

163. Savelyev A, MacKerell AD Jr (2014) All-atom polarizable force field for DNA based on the classical drude oscillator model. J Comput Chem 35:1219–1239 [PubMed: 24752978]

164. Savelyev A, MacKerell AD Jr (2014) Balancing the Interactions of Ions, Water, and DNA in the Drude Polarizable Force Field. J Phys Chem B 118:6742–6757 [PubMed: 24874104]

165. Lemkul JA, MacKerell AD Jr (2017) Polarizable Force Field for DNA Based on the Classical Drude Oscillator: I. Refinement Using Quantum Mechanical Base Stacking and Conformational Energetics. J Chem Theory Comput 13:2053–2071 [PubMed: 28399366]

166. Lemkul JA, MacKerell AD Jr (2017) Polarizable Force Field for DNA Based on the Classical Drude Oscillator: II. Microsecond Molecular Dynamics Simulations of Duplex DNA. J Chem Theory Comput 13:2072–2085 [PubMed: 28398748]

167. Li H, Chowdhary J, Huang L, He X, MacKerell AD Jr, Roux B (2017) Drude Polarizable Force Field for Molecular Dynamics Simulations of Saturated and Unsaturated Zwitterionic Lipids. J Chem Theory Comput 13:4535–4552 [PubMed: 28731702]

168. Huang J, MacKerell AD Jr (2014) Induction of Peptide Bond Dipoles Drives Cooperative Helix Formation in the (AAQAA)3 Peptide. Biophys J 107:991–997 [PubMed: 25140435]

169. Lemkul JA, Savelyev A, MacKerell AD Jr (2014) Induced Polarization Influences the Fundamental Forces in DNA Base Flipping. J Phys Chem Lett 5:2077–2083 [PubMed: 24976900]

170. Savelyev A, MacKerell AD Jr (2015) Competition among Li+, Na+, K+, and Rb+ Monovalent Ions for DNA in Molecular Dynamics Simulations Using the Additive CHARMM36 and Drude Polarizable Force Fields. J Phys Chem B 119:4428–4440 [PubMed: 25751286]

171. Klauda JB, Wu X, Pastor RW, Brooks BR (2007) Long-Range Lennard-Jones and Electrostatic Interactions in Interfaces: Application of the Isotropic Periodic Sum Method. J Phys Chem B 111:4393–4400 [PubMed: 17425357]

172. Leonard AN, Simmonett AC, Pickard FC, Huang J, Venable RM, Klauda JB, Brooks BR, Pastor RW (2018) Comparison of Additive and Polarizable Models with Explicit Treatment of Long-

Range Lennard-Jones Interactions Using Alkane Simulations. J Chem Theory Comput 14:948–958 [PubMed: 29268012]

173. Wennberg CL, Murtola T, Páll S, Abraham MJ, Hess B, Lindahl E (2015) Direct-Space Corrections Enable Fast and Accurate Lorentz–Berthelot Combination Rule Lennard-Jones Lattice Summation. J Chem Theory Comput 11:5737–5746 [PubMed: 26587968]
174. van Erp TS, Meijer EJ (2003) Ab initio molecular dynamics study of aqueous solvation of ethanol and ethylene. J Chem Phys 118:8831–8840
175. Whitfield TW, Martyna GJ, Allison S, Bates SP, Vass H, Crain J (2006) Structure and Hydrogen Bonding in Neat N-Methylacetamide: Classical Molecular Dynamics and Raman Spectroscopy Studies of a Liquid of Peptidic Fragments. J Phys Chem B 110:3624–3637 [PubMed: 16494418]
176. Kirkwood JG (1939) The Dielectric Polarization of Polar Liquids. J Chem Phys 7:911–919
177. Tran HT, Mao A, Pappu RV (2008) Role of Backbone−Solvent Interactions in Determining Conformational Equilibria of Intrinsically Disordered Proteins. J Am Chem Soc 130:7380–7392 [PubMed: 18481860]
178. Salonen LM, Ellermann M, Diederich F (2011) Aromatic Rings in Chemical and Biological Recognition: Energetics and Structures. Angew Chem Int Ed 50:4808–4842
179. Asif M (2017) A Mini Review: Biological Significances of Nitrogen Hetero Atom Containing Heterocyclic Compounds. Int J Bioorganic Chem 2:146
180. Levitt M, Perutz MF (1988) Aromatic rings act as hydrogen bond acceptors. J Mol Biol 201:751–754 [PubMed: 3172202]
181. Suzuki S, Green PG, Bumgarner RE, Dasgupta S, Goddard WA, Blake GA (1992) Benzene Forms Hydrogen Bonds with Water. Science 257:942–945 [PubMed: 17789637]
182. Orabi EA, Lamoureux G (2012) Cation−π and π–π Interactions in Aqueous Solution Studied Using Polarizable Potential Models. J Chem Theory Comput 8:182–193 [PubMed: 26592880]
183. Sperry JB, Wright DL (2005) Furans, thiophenes and related heterocycles in drug discovery. Curr Opin Drug Discov Devel 8:723–740
184. Schnitzer TJ, Truitt K, Fleischmann R, Dalgin P, Block J, Zeng Q, Bolognese J, Seidenberg B, Ehrich EW (1999) The safety profile, tolerability, and effective dose range of rofecoxib in the treatment of rheumatoid arthritis. Clin Ther 21:1688–1702 [PubMed: 10566565]
185. Feng M, Tang B, Liang SH, Jiang X (2016) Sulfur Containing Scaffolds in Drugs: Synthesis and Application in Medicinal Chemistry. Curr Top Med Chem 16:1200–1216 [PubMed: 26369815]
186. Harrold MW, Zavod RM (2014) Basic Concepts in Medicinal Chemistry. Drug Dev Ind Pharm 40:988–988
187. Hernandes M, Cavalcanti SM, Moreira DR, de Azevedo Junior W, Leite AC (2010) Halogen Atoms in the Modern Medicinal Chemistry: Hints for the Drug Design. Curr Drug Targets 11:303–314 [PubMed: 20210755]
188. Xu Z, Yang Z, Liu Y, Lu Y, Chen K, Zhu W (2014) Halogen Bond: Its Role beyond Drug–Target Binding Affinity for Drug Discovery and Development. J Chem Inf Model 54:69–78 [PubMed: 24372485]
189. Auffinger P, Hays FA, Westhof E, Ho PS (2004) Halogen bonds in biological molecules. Proc Natl Acad Sci U S A 101:16789–16794 [PubMed: 15557000]
190. Scholfield MR, Zanden CMV, Carter M, Ho PS (2013) Halogen bonding (X-bonding): A biological perspective. Protein Sci Publ Protein Soc 22:139–152
191. Cavallo G, Metrangolo P, Milani R, Pilati T, Priimagi A, Resnati G, Terraneo G (2016) The Halogen Bond. Chem Rev 116:2478–2601 [PubMed: 26812185]
192. Zhou P-P, Qiu W-Y, Liu S, Jin N-Z (2011) Halogen as halogen-bonding donor and hydrogen-bonding acceptor simultaneously in ring-shaped H3N·X(Y)·HF (X = Cl, Br and Y = F, Cl, Br) Complexes. Phys Chem Chem Phys 13:7408–7418 [PubMed: 21423995]
193. Politzer P, Murray JS, Clark T (2013) Halogen bonding and other σ-hole interactions: a perspective. Phys Chem Chem Phys 15:11178–11189 [PubMed: 23450152]
194. Lu Y, Wang Y, Xu Z, Yan X, Luo X, Jiang H, Zhu W (2009) C−X···H Contacts in Biomolecular Systems: How They Contribute to Protein−Ligand Binding Affinity. J Phys Chem B 113:12615–12621 [PubMed: 19708644]

195. Lu Y, Wang Y, Zhu W (2010) Nonbonding interactions of organic halogens in biological systems: implications for drug discovery and biomolecular design. Phys Chem Chem Phys 12:4543–4551 [PubMed: 20428531]
196. Singh SK, Yamashita A, Gouaux E (2007) Antidepressant binding site in a bacterial homologue of neurotransmitter transporters. Nature 448:952–956 [PubMed: 17687333]
197. Tomar D, Khan T, Singh RR, Mishra S, Gupta S, Surolia A, Salunke DM (2012) Crystallographic Study of Novel Transthyretin Ligands Exhibiting Negative-Cooperativity between Two Thyroxine Binding Sites. PLOS ONE 7:e43522 [PubMed: 22973437]
198. Verschueren KHG, Seljée F, Rozeboom HJ, Kalk KH, Dijkstra BW (1993) Crystallographic analysis of the catalytic mechanism of haloalkane dehalogenase. Nature 363:693–698 [PubMed: 8515812]
199. Tipparaju SK, Mulhearn DC, Klein GM, et al. (2008) Design and Synthesis of Aryl Ether Inhibitors of the Bacillus Anthracis Enoyl-ACP Reductase. ChemMedChem 3:1250–1268 [PubMed: 18663709]
200. Carbone V, Chung R, Endo S, Hara A, El-Kabbani O (2008) Structure of aldehyde reductase in ternary complex with coenzyme and the potent 20α-hydroxysteroid dehydrogenase inhibitor 3,5-dichlorosalicylic acid: Implications for inhibitor binding and selectivity. Arch Biochem Biophys 479:82–87 [PubMed: 18782556]
201. Clark T, Hennemann M, Murray JS, Politzer P (2006) Halogen bonding: the σ-hole. J Mol Model 13:291–296 [PubMed: 16927107]
202. Politzer P, Murray JS, Clark T (2010) Halogen bonding: an electrostatically-driven highly directional noncovalent interaction. Phys Chem Chem Phys 12:7748–7757 [PubMed: 20571692]
203. Nunes R, Costa PJ (2017) Ion-Pair Halogen Bonds in 2-Halo-Functionalized Imidazolium Chloride Receptors: Substituent and Solvent Effects. Chem – Asian J 12:586–594 [PubMed: 28052536]
204. Lin F-Y, MacKerell AD Jr (2017) Do Halogen–Hydrogen Bond Donor Interactions Dominate the Favorable Contribution of Halogens to Ligand–Protein Binding? J Phys Chem B 121:6813–6821 [PubMed: 28657759]
205. Carter M, Rappé AK, Ho PS (2012) Scalable Anisotropic Shape and Electrostatic Models for Biological Bromine Halogen Bonds. J Chem Theory Comput 8:2461–2473 [PubMed: 26588975]
206. Lamoureux G, MacKerell AD Jr, Roux B (2003) A simple polarizable model of water based on classical Drude oscillators. J Chem Phys 119:5185–5197
207. Soteras Gutiérrez I, Lin F-Y, Vanommeslaeghe K, Lemkul JA, Armacost KA, Brooks CL III, MacKerell AD Jr (2016) Parametrization of halogen bonds in the CHARMM general force field: Improved treatment of ligand–protein interactions. Bioorg Med Chem 24:4812–4825 [PubMed: 27353885]
208. Dang LX (1992) Development of nonadditive intermolecular potentials using molecular dynamics: Solvation of Li+ and F− ions in polarizable water. J Chem Phys 96:6970–6977
209. Chang T-M, Dang LX (1997) Ion Solvation in Polarizable Chloroform: A Molecular Dynamics Study. J Phys Chem B 101:10518–10526
210. Dang LX (2000) Molecular dynamics study of benzene–benzene and benzene–potassium ion interactions using polarizable potential models. J Chem Phys 113:266–273
211. Sun X, Chang T, Cao Y, Niwayama S, Hase WL, Dang LX (2009) Solvation of Dimethyl Succinate in a Sodium Hydroxide Aqueous Solution. A Computational Study. J Phys Chem B 113:6473–6477 [PubMed: 19402729]
212. Baer M, Mundy CJ, Chang T-M, Tao F-M, Dang LX (2010) Interpreting Vibrational Sum-Frequency Spectra of Sulfur Dioxide at the Air/Water Interface: A Comprehensive Molecular Dynamics Study. J Phys Chem B 114:7245–7249 [PubMed: 20446719]
213. Dang LX, Truong TB, Ginovska-Pangovska B (2012) Note: Interionic potentials of mean force for Ca2+-Cl− in polarizable water. J Chem Phys 136:126101
214. Brooks BR, Brooks CL, MacKerell AD, et al. (2009) CHARMM: the biomolecular simulation program. J Comput Chem 30:1545–614 [PubMed: 19444816]

215. Brooks BR, Bruccoleri RE, Olafson DJ, States DJ, Swaminathan S, Karplus M (1983) CHARMM: A Program for Macromolecular Energy, Minimization, and Dynamics Calculations. J Comput Chem 4:187–217

216. MacKerell AD Jr, Brooks CL III, Nilsson L, Roux B, Won Y, Karplus M (1998) CHARMM: The Energy Function and Its Parameterization with an Overview of the Program In: Schleyer P v. R, Allinger N, Clark T, Gasteiger J, Kollman PA, Schaefer HF III, Schreiner PR (eds). John Wiley & Sons: Chichester, pp 271–277

217. Phillips JC (2005) Scalable molecular dynamics with NAMD. J Comput Chem 26:1781–1802 [PubMed: 16222654]

218. Jiang W, Hardy DJ, Phillips JC, MacKerell AD Jr, Schulten K, Roux B (2011) High-Performance Scalable Molecular Dynamics Simulations of a Polarizable Force Field Based on Classical Drude Oscillators in NAMD. J Phys Chem Lett 2:87–92 [PubMed: 21572567]

219. Sherwood P, de Vries AH, Guest MF, et al. (2003) QUASI: A general purpose implementation of the QM/MM approach and its application to problems in catalysis. J Mol Struct THEOCHEM 632:1–28

220. Huang J, Lemkul JA, Eastman PK, MacKerell AD (2018) Molecular dynamics simulations using the drude polarizable force field on GPUs with OpenMM: Implementation, validation, and benchmarks. J Comput Chem doi: 10.1002/jcc.25339

221. Abraham MJ, Murtola T, Schulz R, Páll S, Smith JC, Hess B, Lindahl E (2015) GROMACS: High performance molecular simulations through multi-level parallelism from laptops to supercomputers. SoftwareX 1–2:19–25

222. Belle DV, Froeyen M, Lippens G, Wodak SJ (1992) Molecular dynamics simulation of polarizable water by an extended Lagrangian method. Mol Phys 77:239–255

223. Albaugh A, Head-Gordon T (2017) A New Method for Treating Drude Polarization in Classical Molecular Simulation. J Chem Theory Comput 13:5207–5216 [PubMed: 28965397]

224. Rysselberghe PV (1931) Remarks concerning the Clausius-Mossotti Law. J Phys Chem 36:1152–1155

225. Darden T, York D, Pedersen L (1993) Particle mesh Ewald: An N·log(N) method for Ewald sums in large systems. J Chem Phys 98:10089–10092

226. Essmann U, Perera L, Berkowitz ML, Darden T, Lee H, Pedersen LG (1995) A smooth particle mesh Ewald method. J Chem Phys 103:8577–8593

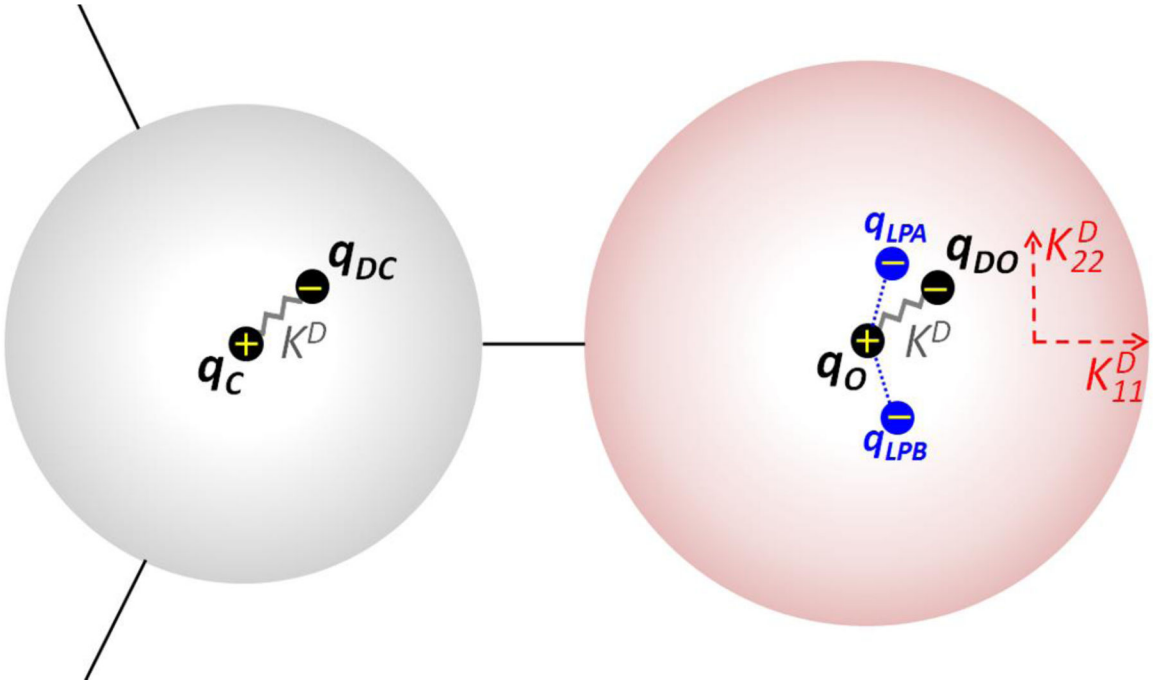

Figure 1.

Schematic of the Drude oscillator model. The addition of Drude particles to carbon (C) and oxygen (O) atoms via harmonic springs with a force constant, K^D, and the subsequent distribution of charge between the atoms (q_C and q_O) and their respective Drude oscillators (q_{DO} and q_{DO}) are presented. Virtual particles to mimic the lone-pairs on the oxygen atom are labeled “LPA” and “LPB” with the charge, q_{LPA} and q_{LPB}. The anisotropic polarization tensor components on the oxygen are labeled as K^D_{11} and K^D_{22}. The other tensor component is orthogonal to K^D_{11} and K^D_{22} and is not shown.

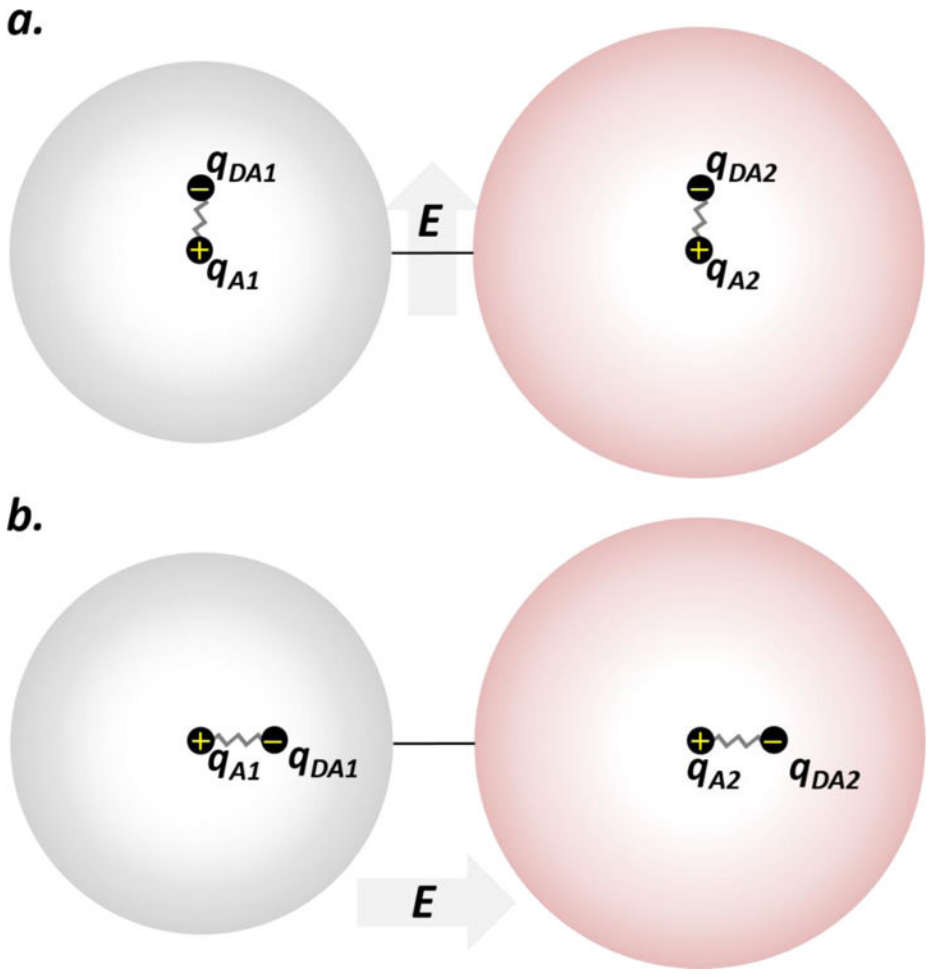

Figure 2.

Schematic illustration of the directional response in the Drude oscillators model under an external electric field, **E**, due to the 1–2 dipole–dipole interactions caused by atom-Drude pairs with charges of q_{A1}–q_{DA1} and q_{A2}–q_{DA2}, respectively. **a.** When **E** is perpendicular to the bond, the 1–2 dipoles damp each other, decreasing the molecular polarizability response perpendicular to the bond. **b.** When **E** is parallel to the bond, the 1–2 dipoles enhance each other thereby increasing the molecular polarizability along with bond.

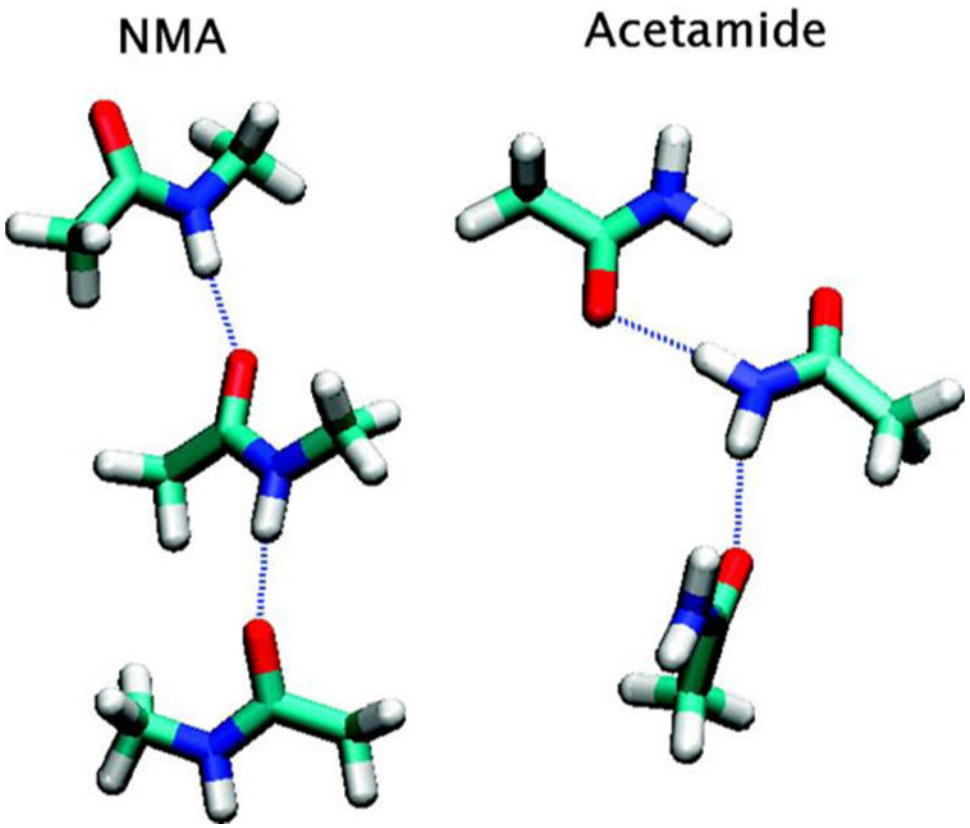

Figure 3.
Representative hydrogen bonding configurations from neat liquid simulations of NMA and acetamide. Reprinted with permission from ref 119. Copyright (2017) American Chemical Society.

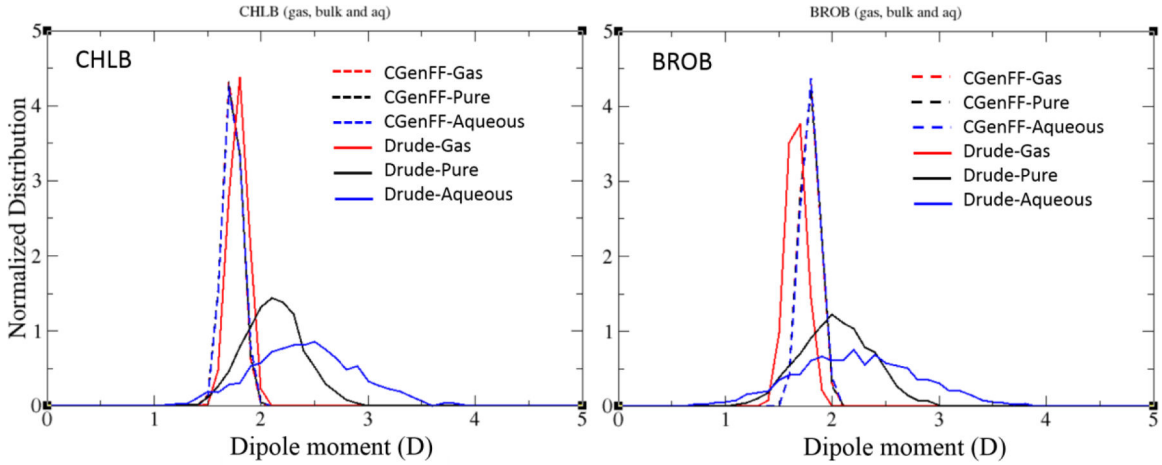

Figure 4.

Dipole moment distributions of chlorobenzene (CHLB) and bromobenzene (BROB) in the gas phase (Gas), in pure solvents (Pure), and in aqueous solution (Aqueous), respectively for both the CGenFF (dotted lines) and Drude (solid lines) polarizable force fields.

Table 1

The scope of available polarizable force fields.

Force Fields	Polarizable models	Scope of Biomolecules
AMBER ff02	Induced Dipole	Proteins [99, 100] Nucleic Acids [99] Atomic ions [96, 98]
AMOEBA	Induced Dipole	Proteins [112] Nucleic Acids * Small molecules [135, 136] Atomic ions [132, 133]
CHARMM-FQ	Fluctuating Charge	Proteins [92, 93] Lipids [127] Carbohydrates [128] Atomic ions [130]
CHARMM Drude	Classical Drude Oscillator	Proteins [162] Nucleic Acids [163–166] Lipids [124, 167] Carbohydrates [158–161] Small molecules [119, 145–157] Atomic ions [47]

* Parameters have not been reported in the literature, but they are available through website at http://dasher.wustl.edu